nanomaterials

MDPI

Review

Recent Progress and Perspectives on Photocathode Materials for CO_2 Catalytic Reduction

Kangli Xu [1,†], Qingming Zhang [1,2,†], Xiaoxia Zhou [1], Min Zhu [2] and Hangrong Chen [1,*]

[1] State Key Laboratory of High-Performance Ceramics and Superfine Microstructure, Shanghai Institute of Ceramics, Chinese Academy of Sciences, Shanghai 200050, China
[2] School of Materials Science and Engineering, University of Shanghai for Science and Technology, Shanghai 200093, China
* Correspondence: hrchen@mail.sic.ac.cn
† These authors contributed equally to this work.

Abstract: The continuous consumption of fossil energy and excessive emissions of carbon dioxide (CO_2) have caused a serious energy crisis and led to the greenhouse effect. Using natural resources to convert CO_2 into fuel or high-value chemicals is considered to be an effective solution. Photoelectrochemical (PEC) catalysis utilizes abundant solar energy resources, combined with the advantages of photocatalysis (PC) and electrocatalysis (EC), to achieve efficient CO_2 conversion. In this review, the basic principles and evaluation criteria, of PEC catalytic reduction to CO_2 (PEC CO_2RR), are introduced. Next, the recent research progress on typical kinds of photocathode materials for CO_2 reduction are reviewed, and the structure–function relationships between material composition/structure and activity/selectivity are discussed. Finally, the possible catalytic mechanisms and the challenges of using PEC to reduce CO_2 are proposed.

Keywords: CO_2 reduction; photoelectrochemical; fuels; photocathode materials

check for updates

Citation: Xu, K.; Zhang, Q.; Zhou, X.; Zhu, M.; Chen, H. Recent Progress and Perspectives on Photocathode Materials for CO_2 Catalytic Reduction. *Nanomaterials* **2023**, *13*, 1683. https://doi.org/10.3390/nano13101683

Academic Editor: Francesc Viñes Solana

Received: 25 April 2023
Revised: 15 May 2023
Accepted: 16 May 2023
Published: 19 May 2023

Copyright: © 2023 by the authors. Licensee MDPI, Basel, Switzerland. This article is an open access article distributed under the terms and conditions of the Creative Commons Attribution (CC BY) license (https://creativecommons.org/licenses/by/4.0/).

1. Introduction

With the increasing demand for energy in modern society, the crisis of fossil fuels (such as oil, natural gas, etc.) and the greenhouse effect have ensued [1–5]. Therefore, the need for the development of clean and renewable energy is urgent. Solar energy, as a kind of renewable, clean energy, has limitless potential [6]. Using solar energy converts carbon dioxide (CO_2) into fuel or high-value chemicals, such as carbon monoxide (CO), formic acid (HCOOH), methanol (CH_3OH), ethanol (CH_3CH_2OH), acetic acid (CH_3COOH), and so on, and is considered an effective means of solving the energy crisis and mitigating the greenhouse effect [7–11].

Photoelectrochemical (PEC) characteristics of semiconductor nanoparticles convert and store solar energy in the form of chemical bonds, making them an effective catalyst for the carbon dioxide reduction reaction (CO_2RR) [12,13]. Compared with photocatalysis (PC) [14,15] or electrocatalysis (EC) [16,17], PEC has obvious advantages in CO_2RR. For instance, PEC CO_2RR can not only promote the separation of photo-generated charges by an external voltage, efficiently overcoming the energy barrier and achieving higher solar energy conversion efficiency [18,19], but can also decrease the overpotential under the action of solar energy to save energy. In other words, the synergistic effects of light and the applied bias potential could jointly reduce the CO_2 activation energy and facilitate the reduction of CO_2 [20].

Generally, PEC CO_2RR includes three processes: (i) the generation of electron-hole pairs on the semiconductor under photo-excitation, and the adsorption of CO_2 on the surface of the catalyst; (ii) the separation and transfer of electron-hole pairs on the semiconductor; (iii) the surface catalytic reaction, including H_2O oxidation by holes and CO_2 reduction by electrons [21,22]. Some *p*-type semiconductor materials have been applied for

PEC CO_2RR, such as CuO_2 [23–25], GaP [26–28], TiO_2 [29,30], etc. An ideal *p*-type semiconductor should meet certain conditions for its conduction band (CB) and valence band (VB) positions, such as the energy level of the CB being more negative than that of CO_2 reduction, and the bandwidth being within the range of light absorption. Although PEC has made significant progress in CO_2RR, there are still significant challenges ahead, mainly including further improving the current density and Faraday efficiency (FE), overcoming the high redox potential to activate CO_2 and break the C=O bond [31,32], and inhibiting the hydrogen evolution reaction (HER) competing with CO_2RR [33].

2. Basic Configuration of PEC Devices

PEC devices for CO_2 reduction are generally divided into two types: single chamber electrolytic cell and H-type electrolytic cell, which are closed containers made of Teflon and quartz glass, respectively.

As shown in Figure 1 [34], in the single-chamber cell, the working electrode, the counter electrode, and the reference electrode are in the same reaction compartment. When CO_2 is reduced, some of the reduction products (such as HCOOH, CH_3OH, etc.) can be transferred to the counter electrode and oxidized, resulting in a significant decline in the yield, which is one of the most fatal drawbacks of the single reactor.

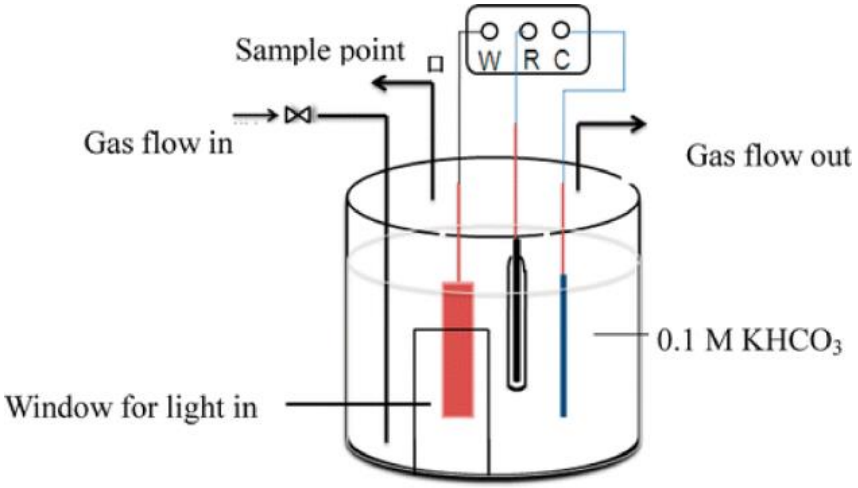


Figure 1. Schematic diagram of the single-chamber reactor. (W, R, and C present the working electrode, reference electrode, and counter electrode, respectively) Adapted with permission from Ref. [34]. Copyright 2014, American Chemical Society.

In the H-type electrolytic cell, the working electrode and the reference electrode are in one compartment, the counter electrode is in another compartment, and the two compartments are separated by a proton membrane. Compared with the single chamber cell, the oxidation reaction occurs in the anode compartment, while the reduction reaction occurs in the cathode compartment, which can effectively prevent the reduction products from being oxidized and can significantly improve the yield of reduction products. However, the transfer of hydrogen protons in the H-type electrolytic cell will be weakened. The three-electrode system of H-type electrolytic cells usually includes the following four types: (1) photocathode (PC, generally *p*-type semiconductor) and dark anode (A, Figure 2a); (2) photoanode (PA, generally *n*-type semiconductor) and dark cathode (C, Figure 2b); (3) PA and PC (Figure 2c); (4) photovoltaic cells and electrodes containing electrochemical catalysts (Figure 2d). Each of the above four electrolytic cells also contains a reference electrode (RE), and the electrolyte can be pure water or a salt solution.

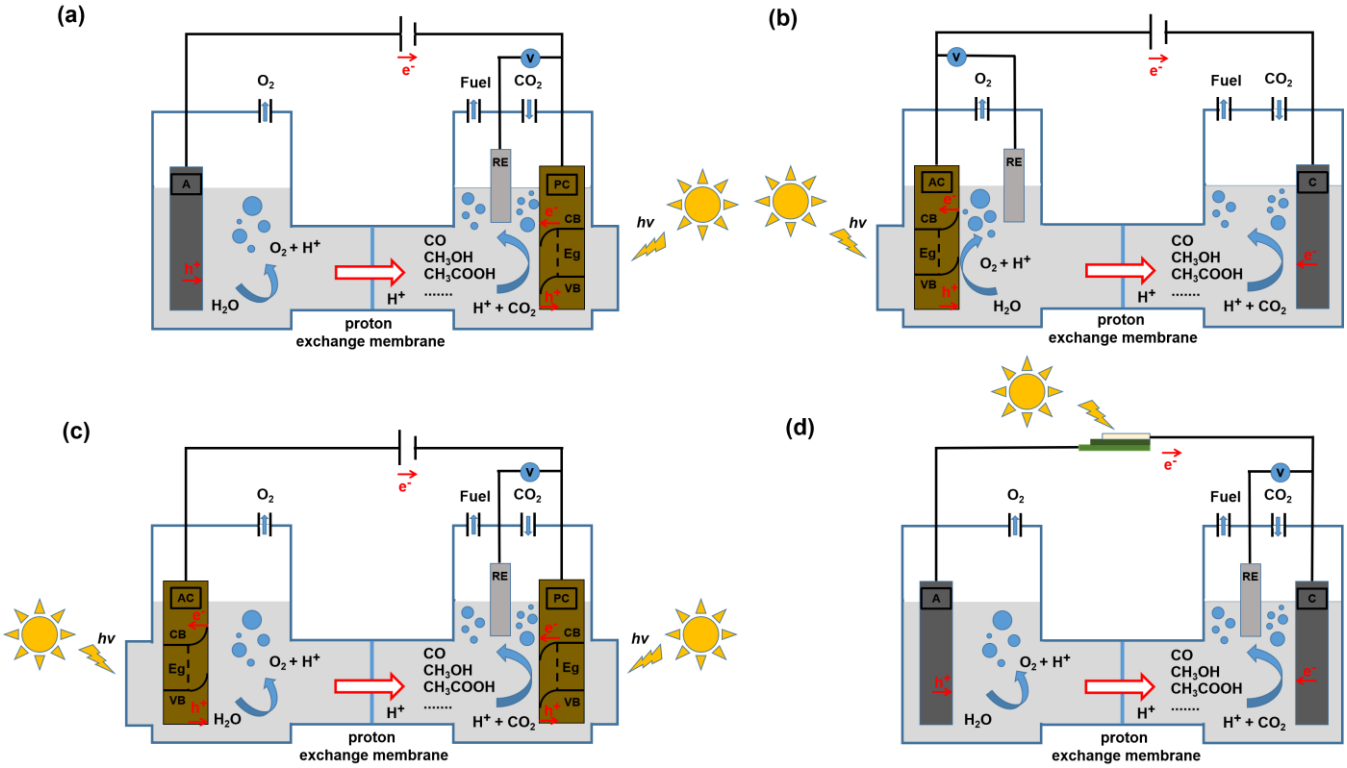


Figure 2. Schematic diagrams of an electrolysis cell for PEC CO_2RR in a three-electrode system. (**a**) PC, A; (**b**) PA, C; (**c**) PA, PC; (**d**) A, C; and each has a RE.

3. General Parameters to Evaluate the PEC CO_2 Reduction

The PEC CO_2RR efficiency on different catalysts can be evaluated by the following specific standards:

3.1. Faraday Efficiency (FE)

FE is one of the important standards to evaluate CO_2 reduction performance, which can be expressed as the ratio of the actual product yield to the theoretical product yield. FE is a more intuitive way to illustrate the selectivity of a catalyst, and its calculation formula is shown in Equation (1) [35–37]:

$$FE_P = \frac{I_P}{I_t} = \frac{n_P\ (\text{mol}) \cdot N \cdot F\ (\text{C/mol})}{Q\ (\text{C})} \quad (1)$$

In Equation (1): FE_p is the Faraday efficiency of p (p represents the reduction product of CO_2, such as HCOOH); I_p is the current density of p; I_t is the total current density. n_p is the amount of the substance; N is the number of electrons that are created for every mole of the corresponding substance. F is Faraday constant (F = 96,485 C/mol). Q is the total amount of charge ($Q = I_t$).

The higher the FE value, the better the selectivity of the catalyst for a specific product. Its value is influenced by multiple factors, such as temperature, electrolyte concentration, applied voltage, solution acidity, and even electrode material purity.

3.2. Solar to Fuel Efficiency (STF)

STF is the conversion efficiency of the PEC reduction of CO_2 system under light irradiation when the action potential between the working electrode and the counter

electrode is zero [38,39]. There are two different calculation methods for STF, such as Equations (2) and (3) [35,38,40]:

$$STF = \frac{C_{fuel}\ (\mathrm{mmol/s}) \cdot \triangle G^0\ (\mathrm{kJ/mol})}{P_{solar}\ (\mathrm{mW/cm^2}) \cdot Area\ (\mathrm{cm^2})} \quad (2)$$

$$STF = \frac{J_{sc}\ (\mathrm{mA/cm^2}) \cdot \triangle E^0(\mathrm{V}) \cdot FE}{P_{solar}\ (\mathrm{mW/cm^2})} \quad (3)$$

In Equation (2): C_{fuel} is the amount of fuel produced per unit of time; ΔG^0 is Gibbs free energy that converts CO_2 into fuel; P_{solar} is the light power density of incident light and *Area* is the effective area of the working electrode exposed by the incident light.

In Equation (3): J_{sc} is photocurrent density under short circuit conditions; ΔE^0 is the thermodynamic potential of CO_2 converted to fuel; *FE* is the Faraday efficiency; P_{solar} is the light power density of incident light.

3.3. Current Density

Current density is the ratio of the tested current to the geometric area of the working electrode, as calculated in Equation (4), which is related to the yield of the product.

$$J_{cd} = \frac{I\ (\mathrm{A}) \cdot 1000}{Area\ (\mathrm{cm^2})} \quad (4)$$

In Equation (4): J_{cd} is current density ($\mathrm{mA/cm^2}$); I (A) represents the total current of the *i-t* test, and *Area* is the geometric area of the working electrode.

Based on the total current density and the FE of the corresponding product (such as HCOOH), the partial current density of the corresponding product can be calculated, as shown in Equation (5).

$$J_{pcd} = J_{cd} \cdot FE_P \quad (5)$$

In Equation (5): J_{pcd} is the partial current density of the corresponding product; FE_p is the Faraday efficiency corresponding to the product.

3.4. Linear Sweep Voltammetry Curve (LSV)

The onset potential and overpotential of the reaction can be obtained from the LSV curve, which is also an important performance for catalysts.

3.5. Incident Photon to Current Efficiency (IPCE)

IPCE is the conversion efficiency of the incident photon into photocurrent under irradiation of incident light with a certain wavelength, which is also called external quantum efficiency [41,42]. IPCE can be calculated by the ratio of the total energy of the converted electrons to the total energy of the incident photons, as shown in Equation (6).

$$IPCE = \frac{1240 \cdot J_{sc}\left(\frac{\mathrm{mA}}{\mathrm{cm^2}}\right)}{\lambda\ (\mathrm{nm}) \cdot P\left(\frac{\mathrm{mW}}{\mathrm{cm^2}}\right)} \quad (6)$$

In Equation (6): J_{sc} is photocurrent density under short circuit conditions; λ is the wavelength of incident light; P is the light intensity of incident light at a certain wavelength.

3.6. Absorbed Photon-Current Conversion Efficiency (APCE)

APCE is the conversion efficiency of absorbed photons into the photocurrent under light irradiation, which can evaluate the recombination efficiency of photo-generated carriers on the semiconductors as shown in Equation (7) [38,43].

$$APCE = \frac{IPCE(\lambda)}{A(\lambda)} \tag{7}$$

In Equation (7): $A(\lambda)$ is the absorbance.

3.7. Turnover Number (TON) and Turnover Frequency (TOF)

TON and TOF are used to characterize the catalytic activity and stability of the catalyst [44]. TON is the mole number of the conversion substrate divided by the mole number of the catalytic activity center, which can also be expressed as the conversion rate of the active site within a certain period. TOF is the number of conversions of a single active site per unit time. In the photoelectrochemical reduction of CO_2, TON and TOF are defined as follows (Equations (8) and (9)) [19,24]:

$$TON = \frac{n_{pro}}{n_{cat}} \tag{8}$$

$$TOF = \frac{n_{pro}}{n_{cat} \cdot t} \tag{9}$$

In Equations (8) and (9), n_{pro} is the mole number of the product; n_{cat} is the mole number of the catalyst; t is reaction time.

3.8. Tafel Slope

Tafel slope reflects the relationship between overpotential and current density. The smaller the Tafel slope, the lower the overpotential under the same kinetic current density, indicating better catalytic performance. Moreover, the Tafel slope is also often used to explain reaction mechanisms [45].

3.9. Reaction Stability

Stability testing is necessary because most semiconductors are unstable due to photocorrosion. The amperometric *i-t* curve is generally used to describe the stability of the catalyst. In the test, when the current density decreases, the stability attenuates.

4. Photocathode Materials for CO_2RR

Generally, CO_2RR involves many proton and electron reactions which can produce various reduction products, including CO, CH_4, HCOOH, CH_3OH, CH_3COOH, CH_3CH_2OH, etc. To date, metal oxides, metal sulfides, phosphates, etc. have been reported as photoelectrochemical catalysts for PEC CO_2RR [46,47]. Moreover, a variety of strategies have been proposed to further improve the activity, stability, and selectivity of the catalyst in PEC CO_2RR, such as the modification of the co-catalyst, and the formation of the protective layer [48]. In this section, we mainly focus on the recent progress of representative photocathode materials to convert CO_2 into different C products, and their performance enhancement strategies.

4.1. Types of Catalysts Commonly Used in PEC CO_2RR

The development core of PEC technology lies in the development of highly active photoelectric-catalysts, and there are many types of catalysts reported so far for CO_2 reduction. Among them, metal/oxides (Pt, Au, Fe_2O_3, $CuFeO_2$, Cu_2O, TiO_2, etc.), metal sulfides (CuS, etc.), metal phosphates (GaP, InP, etc.), MOF-based materials (ZIF9-Co_3O_4, etc.), and non-metallic carbon materials (g-C_3N_4, etc.) have been widely studied. To overcome the overpotential for CO_2 reduction and drive the reaction with sufficient electrical potential,

the conduction band edge of the semiconductor should be much more negative than the potential for CO_2 reduction. Due to the sufficient negative CB positions, II-VI group materials in the periodic table have received extensive research in the early stages, mainly focusing on the properties of quantum dot materials such as CdTe, ZnTe, CdSe, and CdSeTe. These catalysts typically also have appropriate band gap width and band guide position, which are beneficial for absorbing visible light and reducing CO_2. In IV group materials, Si has good absorption of ultraviolet light, visible light, and even infrared light. Although the bandgap position of Si satisfies the multi-electron reduction potential of CO_2RR, it is easily oxidized and the recombination probability of photogenerated carriers is high, making it often used as a substrate. Apart from Si-based catalysts, GaP, InP, Cu_2O, and $CuFeO_2$ are also usually adopted as photocathode substrates.

Based on different semiconductors and reaction systems, the products of PEC CO_2RR also gradually shift from C_1 products (CH_4, CH_3OH, CO, HCOOH, etc.) to C_2 products (C_2H_4, CH_3CH_2OH, CH_3COOH, etc.) and multicarbon (C_{2+}) products (acetone, polyols, etc.). Table 1 summarizes the representative catalysts or active sites for PEC CO_2 reduction according to the types of CO_2-reduced products [49]. Similar to the situation in electrocatalytic CO_2 reduction, Au, Ag-based and Bi, Sn, In-based materials are excellent catalysts for the photocatalytic reduction of CO_2 to CO and HCOOH in aqueous electrolytes, respectively. The highest FEs for PEC CO and HCOOH production, using these metal-based catalysts, are close to 100%. For example, Fe-based catalysts have been studied extensively for CO_2RR. The element dopants, together with the local coordination environment of the Fe center, play remarkable roles in affecting the electronic structures and catalytic performances [50]. The reported Fe-based catalysts mainly produce CO with high Fes up to 90% [51–53]. However, there are few reports about the selective formation of multicarbon (C_{2+}) products over Fe-based catalysts, due to their low FE and low current density. As a comparison, though Cu-based electrocatalysts exhibit unique advantages in electrocatalytic CO_2 reduction, as they can reduce CO_2 to various carbon products (CH_3OH, CH_4, or C_{2+} chemicals) through multiple electron transfer reactions, it is still a huge challenge to improve the selectivity of a single product, due to the complex and diverse properties. Biological catalysts, including molecular catalysts and enzymes, are also applied in PEC CO_2 reduction, where the corresponding photocathodes have achieved a record FE of 100% for CO or HCOOH production [54]. In recent years, graphitic carbon nitride (g-C_3N_4), as a non-metallic semiconductor material, has shown broad application prospects in CO_2 reduction research, due to its excellent catalytic performance, which comes from its sufficiently negative CB. Research has shown that pyridine N enriched g-C_3N_4, as an active site, can contribute to C-C coupling in PEC CO_2RR to produce CH_3CH_2OH. In addition, vacancy-rich TiO_2 [55], oxygen-doped CdS, $CuFeO_2$, and carbon/Cu_2O composites are also explored as active sites for PEC CO_2 reduction to produce CH_3OH, CH_3COOH, or CH_3CH_2OH, but most of them showed low selectivity for their primary products during the PEC CO_2 reduction process. To sum up, it remains a significant challenge for electrocatalytic CO_2RR to produce C_{2+} products efficiently over non-copper catalysts, and there is a lack of photocathodes using metal-based or biological co-catalysts for PEC CO_2 reduction to produce CH_3OH, CH_4, or C_{2+} chemicals with high FEs (>90%).

Table 1. Summary of the catalysts or active sites for PEC CO_2 reduction to different products.

Products	Cocatalysts or Active Sites
H_2	Pt, Ni, Si, etc.
CO	Au, Ag, Pt-TiO_2, $CuAu_3$, AgP_2, $Cu(btc)_3$, ZnO, ZnTe, etc.
HCOOH	Sn, Bi, In, CuS, RuCt, FDH enzyme, $CuFeO_2$, Co_3O_4, etc.
CH_3OH	TiO_2, TiO_2-Cu^+, O-doped Cds, etc.
CH_4	GaN/Cu, GaN/CuFe, Cu-Ag, etc.
CH_3COOH	$CuFeO_2$, etc.
C_2H_4 (g)	Cu, Ag/Cu_2O in AcCN, etc.
CH_3CH_2OH	Carbon/Cu_2O composite, N, O-doped Cds, g-C_3N_4, etc.

4.2. Strategies for Enhancing the Performance of Photocathodes in PEC CO_2RR

In recent years, numerous achievements have been made in the research of photocatalytic CO_2 reduction in photocathode materials. Despite significant progress, there are still many challenges in the efficient reduction of the CO_2 reaction process. This review is based on the aforementioned PEC CO_2RR process and briefly elaborates on the basic strategies for enhancing the efficiency of PEC CO_2RR from three perspectives: light absorption, carrier separation, and surface reaction kinetics.

4.2.1. Improving Light Absorption

The light absorption capacity of semiconductors is closely related to their band structure, therefore, optimizing the band structure of semiconductors is a major strategy for enhancing the absorption performance of photocathodes. In addition, loading light absorbing material onto catalysts is an effective method to enhance their light absorption performance.

Self-doping or doping with other elements can alter the band structure of catalytic materials, thereby improving their light absorption performance. At the same time, the conductivity of the photocathodes is greatly improved, and the current density increases. With regard to PEC systems, there are only a few studies on the doping of photoelectrodes, including Mg-doped $CuFeO_2$ [56], B-doped C_3N_4 [57], N-doped ZnTe [58], and S, N-co-doped nanoporous carbon [59] photocathodes for PEC reduction of CO_2.

Plasma metal nanostructures can also improve the efficiency of light energy collection and energy conversion, and have been widely used in semiconductors [60]. Under the action of an incident light wave electric field, the outer free electrons of metal nanoparticles are polarized and move, generating a new electric field that applies a linear internal restoring force within the original system. This type of electronic dipole oscillation, limited to the interior of metal nanoparticles, is known as localized surface plasmon resonance (LSPR). Common precious metals with LSPR effects include Au, Ag, Pt, etc., while non-precious metals mainly include Cu. In catalytic reactions, the abovementioned metal cocatalysts exhibit excellent performance in PEC CO_2RR.

Incorporating dye molecules and quantum dots into the catalyst can enhance its light absorption ability. Xu et al. [30] utilized multifunctional TiO_2 thin films as photocathodes to convert CO_2 into CO, and lower CH_3CH_2OH through PEC. The light absorption ability of the photocathodes is improved by combining the dye molecule, Eosin Y Disodium, with TiO_2, and Pd nanoparticles and amine ligands are introduced to capture protons and CO_2, respectively.

4.2.2. Enhancing the Separation Efficiency of Photogenerated Carriers

In the process of PEC CO_2 reduction, a large amount of recombination of photogenerated carriers occurs on the catalyst body and surface, greatly reducing the catalytic reaction efficiency. Therefore, enhancing the separation efficiency of photogenerated carriers is an important means of improving the photoelectrocatalytic efficiency.

Constructing homo/heterojunctions is considered a highly effective strategy for improving the separation of photogenerated electrons and holes, as well as enhancing the selectivity for specific products in PEC CO_2 reduction [61]. The heterojunction photocathode is usually composed of two or more semiconductors with alternating band structures, such as ZnO/ZnTe [62], CdTe/ZnTe [63], CuO/Cu_2O [64], and $CuFeO_2$/CuO [65], etc.

4.2.3. Accelerating Surface Reaction Kinetics

Interface reaction is a crucial step in the PEC process. As mentioned above, after the generation and separation of photogenerated carriers, they ultimately need to be transferred to the surface of the catalyst to participate in the redox reaction. For the photoelectric reduction of the CO_2 system, when the photogenerated carriers reach the catalyst surface, electrons participate in the CO_2RR, and holes participate in the oxidation reaction of H_2O. Research has shown that strengthening the interface reaction process is crucial for improving the efficiency of PEC CO_2RR.

Controlling the surface morphology of catalysts is an effective way to accelerate interfacial reactions. By adjusting the surface morphology of the catalyst, it has a high specific surface area and exposes a specific crystal plane, thus promoting the absorption of CO_2 at its surface active site. In addition, precise control of the morphology of the co catalyst can be an effective method to ensure illumination on the photocathode.

Modifying semiconductor surfaces, using different techniques, is another effective strategy for accelerating interface reactions. The sluggish reaction kinetics of CO_2 reduction, as a result of the high activation energy or overpotential, largely impedes the reaction process. By using techniques such as chemical etching, electrochemical treatment, or chemical vapor deposition (CVD), catalyst deposition (noble/non-noble metals, MOFs [66], molecular complexes [67], polymers, carbon materials [68]), and passivation with thin protective materials on the surface of photocathodes, the surface of photocathodes can be functionalized, which help to accelerate interface reaction kinetics (accelerate multi-electron reactions, reduce reaction overpotential, and promote the transfer of photogenerated charge carriers to the catalyst surface). In some cases, surface catalysts can also improve the stability of the photoelectrodes by rapidly consuming the surface charge carriers. Furthermore, specific functional catalysts can increase the selectivity for the desired products by manipulating the adsorption strengths of certain reaction intermediates.

4.3. Representative Photocathode Materials and Their Performance Enhancement Strategies

4.3.1. Zinc (Zn)-Based Photocathodes

Zinc-based photocathodes, such as ZnTe and ZnO, used in PEC CO_2RR, mainly produce CO. ZnTe is a p-type semiconductor with a direct bandgap of 2.3 eV, and the conduction band position of ZnTe is relatively negative, which is conducive to transport interface electrons [69,70]. Jang et al. [71] first reported a new Zn/ZnO/ZnTe photocathode for PEC CO_2RR (Figure 3a). An obvious photoelectric reaction can be observed on the Zn/ZnO/ZnTe photocathode, and under the Hg lamp (with >420 nm cutoff filter), the photocurrent density of the Zn/ZnO/ZnTe photocathode approaches 20 $mA{\cdot}cm^{-2}$ at −0.7 V vs. the reversible hydrogen electrode (RHE) (Figure 3b). Compared with Zn/ZnO, Zn/ZnO/ZnTe showed significantly improved visible light absorption performance, which is consistent with the result that the light absorption edge can be extended to approximately 570 nm (Figure 3c) [62]. However, due to the competitive reaction of HER, the FE of CO at −0.7 V vs. RHE is as low as 22.9%, and the stability of the Zn/ZnO/ZnTe photocathode also needs to be enhanced. To further improve its performance, Jang et al. coupled Au nanoparticles with ZnTe/ZnO/Zn (ZOZT) to obtain a ZOZT-Au photocathode, as shown in Figure 3d. ZOZT-Au not only further enhanced photocurrent density, but also improved the FE of CO to 58% at −0.7 V vs. RHE, in comparison with ZOZT (Figure 3e–f).

This work offers an effective strategy by using a highly conductive metal substrate and heterojunction structure, which can improve the current density and facilitate the separation of photogenerated carriers. In particular, the deposition of Au nanoparticles could further improve the selectivity for CO and inhibit the competitive H_2 evolution, as well as promote the electron transfer by forming a Schottky junction with ZnTe at the interface. In addition, Au enhances the stability of the electrode. Coupling metal electrocatalysts with semiconductors or forming heterojunctions between semiconductors can effectively increase current density and promote carrier separation, which is worth learning in the design of optoelectronic materials.

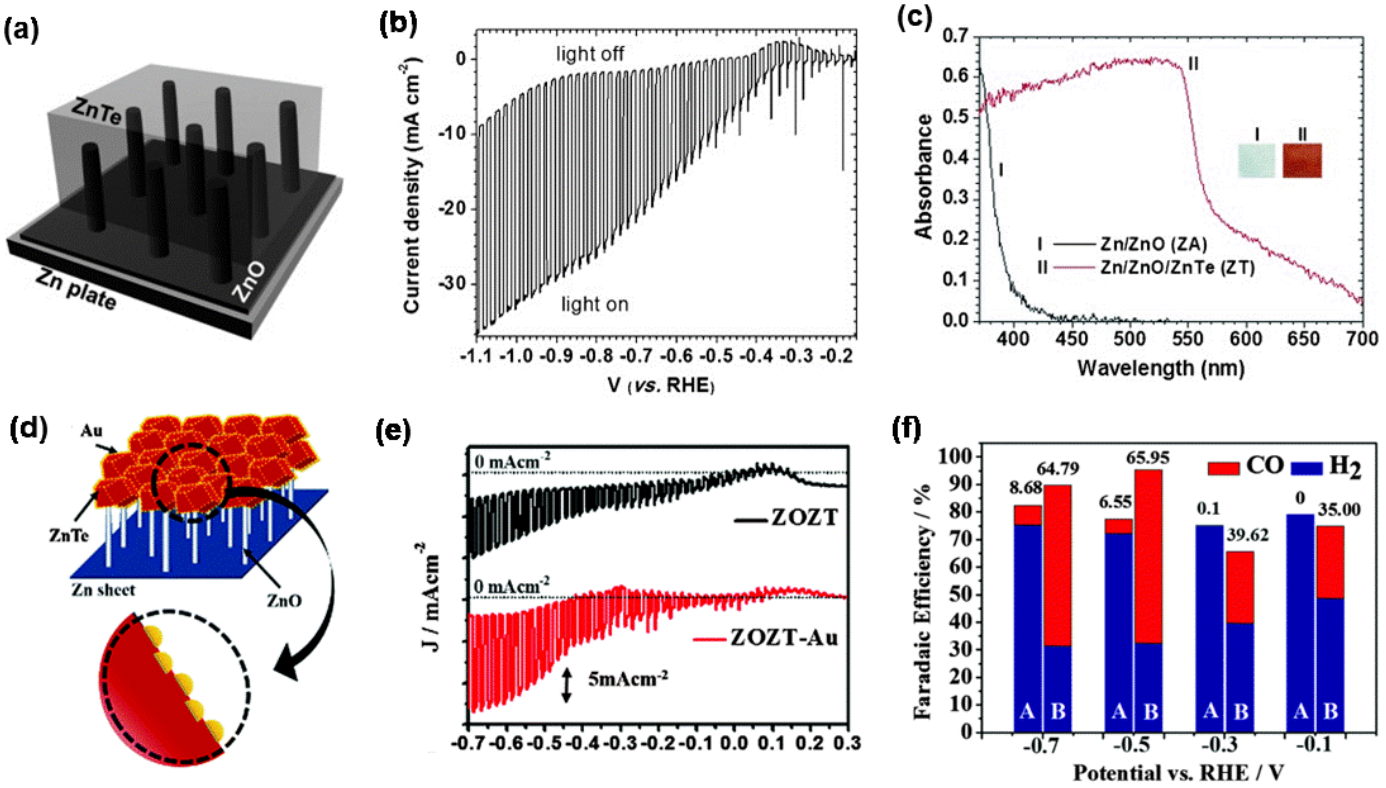


Figure 3. (**a**) Diagram of the Zn/ZnO/ZnTe structure; (**b**) LSV curves of Zn/ZnO/ZnTe with the light on and off; (**c**) UV-Vis absorption spectra of Zn/ZnO and Zn/ZnO/ZnTe. Adapted with permission from Ref. [71]. Copyright 2014, Wiley-VCH. (**d**) Diagram of Au-coupled ZnTe/ZnO/Zn structure; (**e**) LSVs of ZOZT and ZOZT-Au with the light on and off; (**f**) FE for ZOZT (A) and ZOZT-Au (B) (the value above the cylinder indicates the selectivity of CO, concerning H_2 during H_2O reduction). Adapted with permission from Ref. [62]. Copyright 2016, Royal Society of Chemistry.

4.3.2. Cobalt (Co)-Based Photocathodes

The most common catalyst in Co-based photocathodes is Co_3O_4, which is also a semiconductor material with a band gap of 2.07 eV and a conduction band of −1.05 eV [72,73], and the appropriate band gap width and band guide position are beneficial for absorbing visible light and reducing CO_2. Zhao et al. carried out a systematic study on Co_3O_4 for PEC CO_2RR. Firstly, the hierarchical porous Co_3O_4 (HA-Co_3O_4) was designed for PEC CO_2RR to HCOOH [74], which showed the top micro-flowers and the bottom rhombus structure (Figure 4a–c). This typical hierarchical structure added the active site of photocatalysis and electrochemistry, making the photocurrent density on the HA-Co_3O_4 electrode much higher than that on the Co_3O_4 rhombus nanorod electrode (NR-Co_3O_4) and the Co_3O_4 nanoparticle-coated electrode (NP-Co_3O_4) (Figure 4d), and the $HCOO^-$ yield reached 384.8 ± 7.4 μmol in 8 h, which is higher than the yield of pure EC, PC and EC + PC (Figure 4e). Secondly, the metal Cu nanoparticles were modified on the Co_3O_4 nanotube arrays to form a metal/metal oxide composite material (Cu-Co_3O_4) for PEC CO_2RR (Figure 4f) [75]. The Co_3O_4 nanotube arrays obtained by in situ growth in cobalt foil, through anodizing technology, can not only reduce the resistance between the substrate and the nanotube arrays, but also provide more active sites to promote light absorption. (Figure 4g). In addition, Cu nanoparticles can also promote the adsorption of reducing intermediates, thereby improving the selectivity of formic acid, resulting in a yield of 6.75 mmol·L^{-1}·cm^{-2} of HCOOH in PEC CO_2RR, with selectivity approaching 100% within 8 h (Figure 4h). The successful application of Cu-Co_3O_4 in PEC CO_2RR once again proves that the coupling between metal and semiconductor is a very desirable design in PEC CO_2RR.

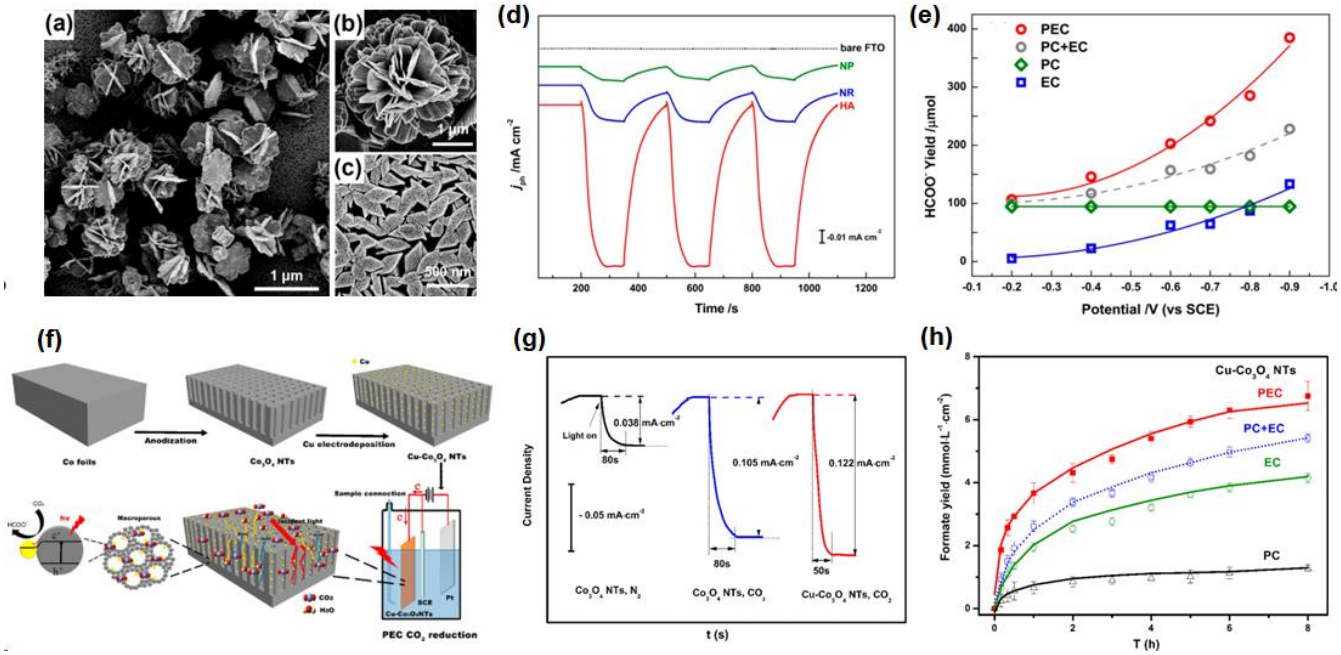


Figure 4. (**a**–**c**) SEM images of HA-Co_3O_4 structure; (**d**) *i-t* curves of bare FTO, NP-Co_3O_4, NR-Co_3O_4, and HA-Co_3O_4 with the light on/off; (**e**) Formate yields of the sample HA-Co_3O_4 in PEC CO_2RR (red circle), EC (blue square), PC (green rhombus) and PC + EC (gray circle). Adapted with permission from Ref. [74]. Copyright 2013, American Chemical Society. (**f**) Schematic mechanism of the Cu-Co_3O_4 NTs fabrication and PEC CO_2RR; (**g**) *i-t* curves of Co_3O_4 NTs and Cu-Co_3O_4 NTs in N_2 and CO_2-saturated electrolyte; (**h**) Formate yields of the sample Cu-Co_3O_4 in PEC CO_2RR (red), EC (green), PC (black) and PC + EC (blue). Adapted with permission from Ref. [75]. Copyright 2015, American Chemical Society.

The composite Ru(bpy)$_2$dppz-Co_3O_4/carbon aerogel (Ru(bpy)$_2$dppz-Co_3O_4/CA) (Figure 5a), prepared by solvothermal reaction and droplet casting method, also showed superior PEC CO_2RR performance [72]. The photocurrent response (Figure 5b) and the yield of $HCOO^-$ (Figure 5c) on the sample Ru(bpy)$_2$dppz-Co_3O_4/CA is significantly higher than that of Co_3O_4 and Co_3O_4/CA, such as the FE of $HCOO^-$ is 86% at −0.6V vs. normal hydrogen electrode (NHE). Such a good activity is mainly ascribed to the following aspects: (1) carbon aerogel has rich micropores and a large specific surface area, which can enhance the adsorption of CO_2; (2) Ru(bpy)$_2$dppz can be used as an electron transfer medium and CO_2 activator, and the synergistic effect between bpy and dppz can also effectively achieve the rapid transfer of electrons. It is believed that modifying the metal/oxide catalysts with organic molecules or linkers, to construct a microenvironment for CO_2 activation and reduction, will be a new strategy to regulate the photocathode activity or product selectivity.

Additionally, the Co_3O_4 nanowires (Co_3O_4 NWs), combined with Co-MOF (ZIF9), are conducive to the adsorption, and the capture of CO_2 has also been applied in PEC CO_2RR (Figure 5d) [76]. Under light illumination, the yield of formic acid is 578.7 mol·L^{-1}·cm^{-2} and the FE of HCOOH is 70.6% in 8 h at −0.9V vs. saturated calomel electrode (SCE) (Figure 5e). DFT theoretical calculation results showed that when CO_2 was absorbed into the micropores of ZIF9, the structure of linear CO_2 would change and the bond angle would reduce, due to bending, which could promote the activation of CO_2 (Figure 5f–g). It has been concluded that the structure of Co_3O_4 NWs can enhance light capture, while ZIF9 can improve the adsorption performance of CO_2. Moreover, the p-p type heterojunction between Co_3O_4 NWs and ZIF9 is highly beneficial in promoting the separation of photogenerated electron-hole pairs, showing great potential in CO_2 reduction. In brief, the research progresses on Co-based photocathodes has paved the way for the development of non-precious metals to achieve PEC reduction of CO_2.

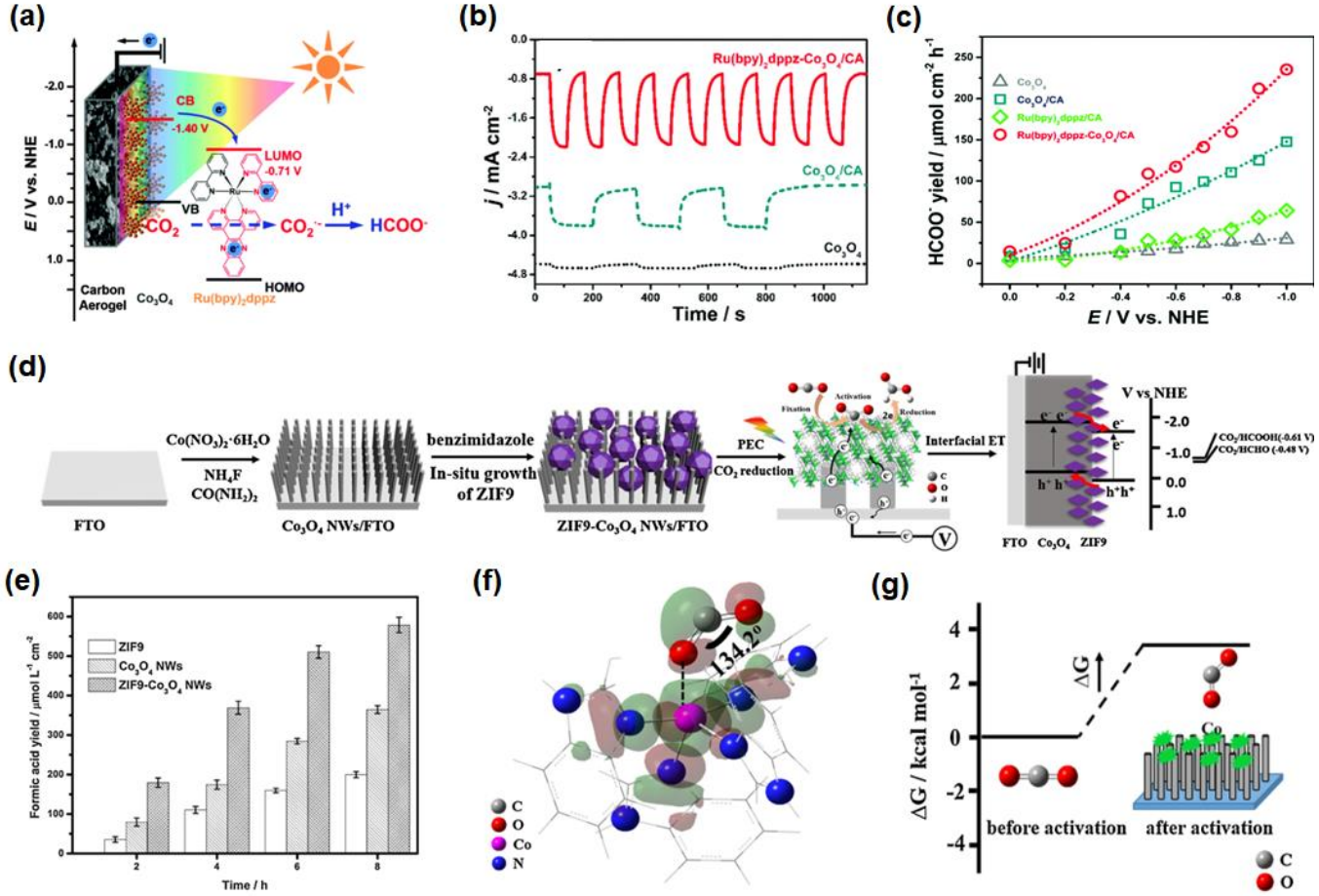


Figure 5. (**a**) Schematic illustration structure of Ru(bpy)$_2$dppz-Co_3O_4/CA and PEC CO_2RR; (**b**) *i-t* curves of Co_3O_4/FTO (dotted line), Co_3O_4/CA (dashed line) and Ru(bpy)$_2$dppz-Co_3O_4/CA (solid line) with the light on and off; (**c**) the yield of $HCOO^-$ on Co_3O_4/FTO (gray triangle), Ru(bpy)$_2$dppz/CA (green rhombus), Co_3O_4/CA (cyan square) and Ru(bpy)$_2$dppz-Co_3O_4/CA (red circle). Adapted with permission from Ref. [72]. Copyright 2016, Royal Society of Chemistry. (**d**) Preparation schematic diagram of ZIF9-Co_3O_4 NWs and proposed mechanism of PEC CO_2RR; (**e**) formate yields on the samples, ZIF9, Co_3O_4 NWs, and ZIF9-Co_3O_4 NWs electrode in PEC CO_2RR; (**f**) SOMO orbit of the bent CO_2-ZIF9 molecule; and (**g**) its corresponding changes in Gibbs energetic Adapted with permission from Ref. [76]. Copyright 2016, Elsevier.

4.3.3. Silicon (Si)-Based Photocathodes

Si, as a potential p-type semiconductor, has a narrow energy bandgap and is widely used in PEC. Moreover, Si is abundant on Earth and has great industrial value [77]. Bradley et al. first reported p-Si photocathode materials in 1982 [78]. In PEC CO_2RR, p-Si is usually used for substrates and compounded with metal or other semiconductor catalysts. This is because, although Si has strong light capture ability, its CO_2 reduction activity is weak and it has high selectivity for hydrogen. It has been reported that Si photoelectrodes modified with nanoporous Au thin film mesh, formed by electrochemical reduction of the anodized gold thin film, can be used for PEC CO_2RR (Figure 6a) [77]. Compared with pure Si photoelectrodes, when the potential is greater than 1.1 V vs. RHE, the photocurrent density of Si photoelectrodes, with nanoporous Au thin film mesh, is reduced, but the initial potential shifts to a positive potential (Figure 6b). Additionally, the FE of CO on Si photoelectrode, with reduced anodic Au (w/RA Au), was 91% at −0.03 V vs. RHE, which is higher than that of pure Si and Si photoelectrode with untreated Au (Figure 6c). The excellent PEC CO_2RR of the w/RA Au was ascribed to the Au co-

catalyst and p-n heterojunctions formed on Si, which jointly facilitated the separation of the photogenerated carrier.

In addition, Choi et al. [79] reported that Ag-assisted etchants were mixed with HF and H_2O_2 to form Si nanowires by etching the Si surface and combined with co-catalyst Sn to convert CO_2 into HCOOH through PEC CO_2RR (Figure 6d). Under AM 1.5G light (100 mW·cm^{-2}), p-Si wire arrays have higher photocurrent density, more positive onset potential, and better stability. As the etching time increases, the photocurrent first increases and then remains unchanged (Figure 6e). The length of nanowires and the coupling of Sn have an effect on the selectivity of PEC CO_2RR (Figure 6f). In addition, the FE for HCOOH in the H-type electrolytic cell reached 88.4%, which is higher than that in the single-chamber electrolytic cell. Although p-Si wire arrays can promote photon absorption and carrier separation, due to their high geometric optical path and low reflectivity, the preparation process generally requires highly corrosive hydrofluoric acid or complex etching technologies, making it unsuitable for large-scale operation.

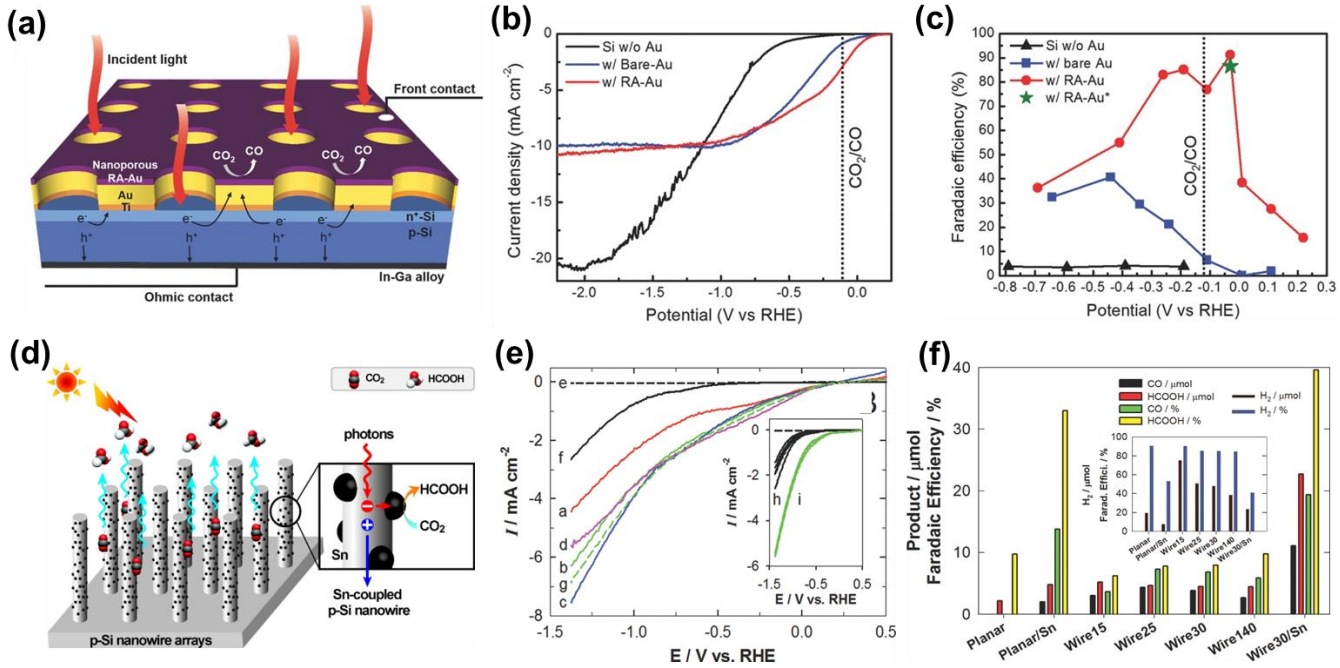


Figure 6. (**a**) Schematic of Au_3Cu NP/Si NW photoelectrode design for CO_2 reduction; (**b**) PEC CO_2RR LSV curves; (**c**) FE of CO; (bare Si—black; Si photoelectrodes of the Au mesh without RA treatment—blue; Si photoelectrode of the Au mesh with RA treatment—red; Green star symbol indicates FE of CO on Si with the Au mesh after the RA treatment). Adapted with permission from Ref. [77]. Copyright 2016, Wiley-VCH. (**d**) Vertically aligned, free-standing p-Si nanowire arrays of varying lengths are grown on p-Si wafers and coupled with Sn nanoparticles for solar CO_2 conversion; (**e**) LSVs of the irradiated p-Si wire arrays etched for 1, 3, 5, and 10 h (a–d, respectively), planar Si (e—dark; f—irradiated), and p-Si wire array coupled with g—Sn nanoparticles. Inset: 5-times repeated LSVs of the h—irradiated planar, and i—wire electrodes; (**f**) Comparison of the products (CO and formate) and their FE. Inset: the amount of H_2 produced and FE. Adapted with permission from Ref. [79]. Copyright 2014, Wiley-VCH.

A p-Si/metal oxide (nitrides)/metal composite was also used for PEC CO_2RR. Sheng et al. [80] photo-deposited ZnO and Cu on the GaN/n$^+$-p Si substrate to convert CO_2 to syngas using PEC, in which the FE of CO was as high as 70% at −0.2 V vs. RHE in CO_2-saturated 0.5 M $KHCO_3$ solution (pH = 8) (Figure 7a–b). The photocurrent density and FE of CO have no obvious attenuations at −0.2 V vs. RHE under illumination for 10 h (Figure 7c), indicating their high stability, mainly ascribed to the photoabsorption of p-n Si heterojunction, effective electron extraction by GaN, and the fast surface

kinetics of the Cu-ZnO co-catalyst. LSV results show that Cu-ZnO/GaN/n^+-p Si has the highest photocurrent density among all presented samples (Figure 7d), which could be attributed to the ZnO as a cocatalyst to absorb and activate CO_2 molecules, leading to the bend of the C=O bond and the decrease in CO_2 chemical stability (Figure 7e). In the Cu-ZnO/GaN/n^+-p Si photocathode, Si serves as the substrate for light capture, and GaN promotes the separation of photogenerated carriers. Combined with the Cu-ZnO cocatalyst, PEC reduction of CO_2 can be effectively achieved, which demonstrates the combination of photocatalysts and electrocatalysts, fully achieving the synergistic effects of photo and electricity in material design.

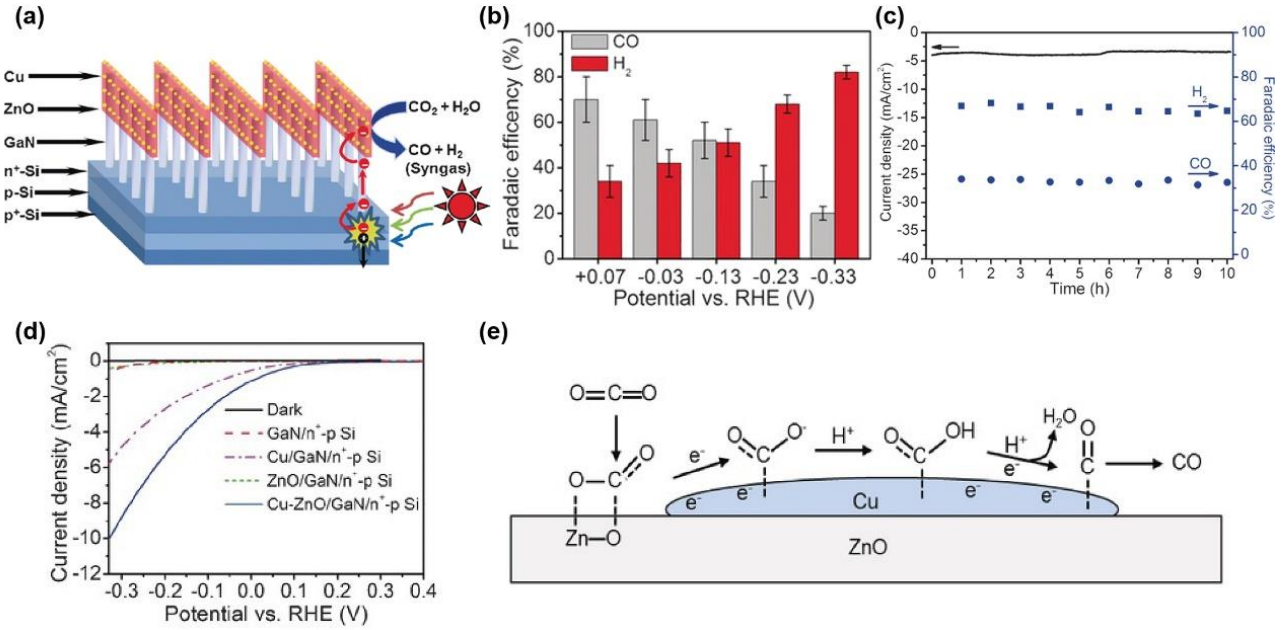


Figure 7. (**a**) Schematic illustration of Cu-ZnO/GaN/n^+-p Si photoelectrode structure and PEC CO_2RR; (**b**) relationship between the FE (CO and H_2) of Cu-ZnO/GaN/ n^+-p Si photocathode and the potential; (**c**) the stability and FE of Cu-ZnO/GaN/n^+-p Si photocathode at −0.2 V vs. RHE for CO and H_2; (**d**) LSV curves of different samples; (**e**) possible reaction mechanism for the PEC CO_2RR to produce CO on Cu-ZnO cocatalysts. Adapted with permission from Ref. [80]. Copyright 2016, Wiley-VCH.

4.3.4. Iron (Fe)-Based Photocathodes

Fe-based photocathode materials mainly include $CuFeO_2$ and Fe_2O_3. Among them, the bandwidth of $CuFeO_2$ is 1.5~1.6 eV, which is beneficial to photon absorption. Furthermore, $CuFeO_2$ has the structure of delafossite, and it has been reported that the conductivity of the delafossite structure can be improved by adding trivalent or bivalent metals [56,81]. For example, Gu et al. [56] synthesized Mg-doped $CuFeO_2$ by traditional solid-state methods, which showed a high photocurrent density. However, the FE of $HCOO^-$ is as low as 10% on the photocathode Mg-doped $CuFeO_2$ at −0.9 V vs. SCE, due to the serious hydrogen evolution competitive reaction. Interestingly, $CuFeO_2$ and CuO mixed p-type catalysts were prepared to improve the PEC CO_2RR activity, and the selectivity of $HCOO^-$ is close to 90% under simulated light irradiation [65]. More importantly, the activity can last for a week. Moreover, the onset potential of $CuFeO_2$/CuO is +0.9 V vs. RHE, which is a very positive potential in PEC CO_2RR.

The bandwidth of transition metal oxide Fe_2O_3 is 2.20 eV, therefore it has good visible light absorption performance [82]. Compared with the pure TiO_2 nanotubes, the TiO_2 nanotubes modified with Fe_2O_3 (Fe_2O_3/TiO_2 NTs) not only expanded the optical absorption region (Figure 8a) but also achieved good PEC CO_2RR for HCOOH [83]. At an incident wavelength of 500 nm and a bias voltage of −1.0 V vs. RHE, the selectivity and

yield of HCOOH can reach 99.89% (Figure 8b) and 74,896.13 nmol·h^{-1}·cm^{-2} (Figure 8c), respectively. As shown in Figure 8d, Fe_2O_3/TiO_2 NTs have an embedded heterojunction, and electrons in the VB of TiO_2 gradually transfer to the CB of Fe_2O_3 under incident light irradiation. Meanwhile, the Fe_2O_3 can absorb CO_2 to form $CO_2^{\cdot-}$ (ads) and further obtain $[Fe^{III}COOH]^{2+}$ under the effect of electrons and H_2O. Finally, the HCOOH was formed during the transformation process of O-Fe^{III} and O-Fe^{II}. Since Fe-based photocathodes are beneficial for future large-scale applications, the development of efficient non-noble-metal-based co-catalysts should receive much more attention.

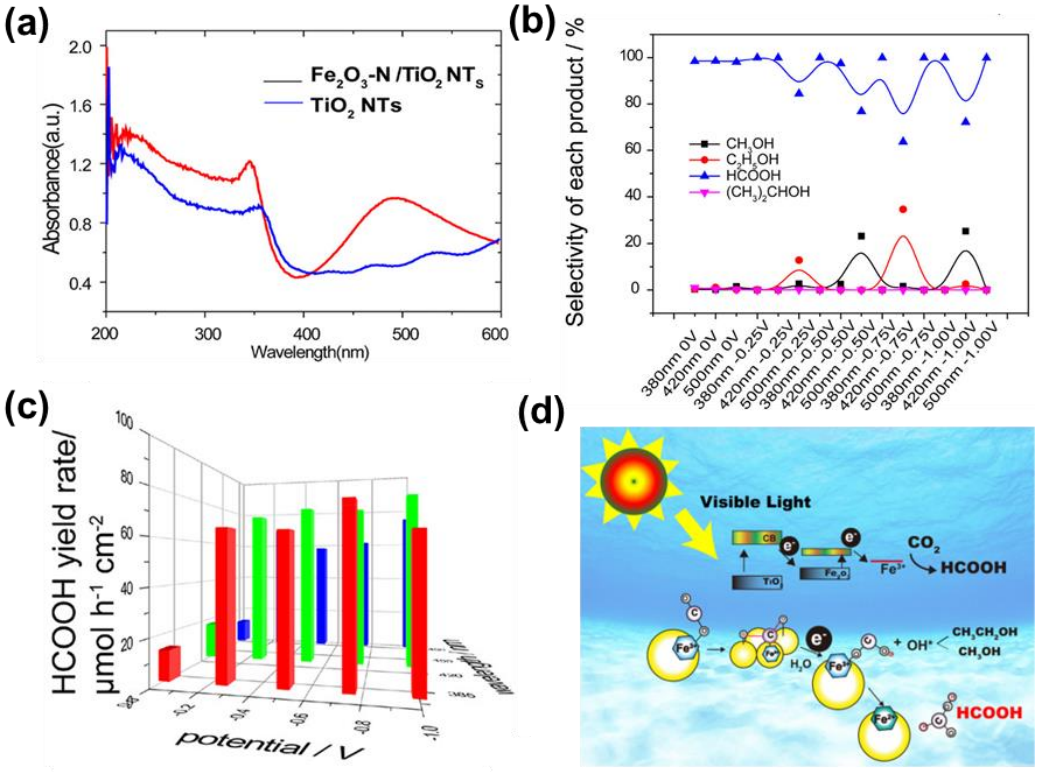


Figure 8. (**a**) UV-DRS of TiO_2 NTs and Fe_2O_3/TiO_2 NTs; (**b**) selectivity of CO_2RR products under PC (0 V) and PEC conditions on $F_{e2}O_3/TiO_2$ NTs; (**c**) yield rate of HCOOH on Fe_2O_3/TiO_2 NTs; (**d**) proposed reaction pathways for the PEC CO_2RR on Fe_2O_3/TiO_2 NTs. Adapted with permission from Ref. [83]. Copyright 2018, American Chemical Society.

4.3.5. Copper (Cu)-Based Photocathodes

Among the non-noble metals, many recent studies on CO_2 reduction have primarily focused on designing Cu-based materials due to their high abundance, low toxicity, unique catalytic activity, and good stability. There are two main forms of copper oxides, CuO and Cu_2O. Cu-based photocathodes, especially Cu_2O, are the most common photoelectrochemical catalysts, due to their good light absorption performance [84,85]. The bandwidth of Cu_2O is 1.9–2.2 eV, and the CB position is conducive to the reduction of CO_2 [86]. Additionally, the maximum photocurrent density of Cu_2O can reach 14.7 mA·cm^{-2} under the illumination of AM 1.5 G light [87]. However, the biggest disadvantage of Cu_2O is its susceptibility to light corrosion. Therefore, heterojunction and core–shell structure, etc. are often used to effectively avoid photo-corrosion. Additionally, CuO has also a narrow bandwidth of 1.3–1.6 eV, leading to a high absorption coefficient in the solar spectrum [88]. Moreover, Cu-based photocathodes have complex and diverse properties, thus it is challenging to improve the selectivity of a single product.

The CuO-Cu_2O nanorod arrays, as a photocathode, have been prepared on a Cu substrate by a thermal oxidized and electrodeposition process for the reduction of CO_2 (Figure 9a) [64]. By changing the time of Cu_2O electrodeposition, the FE of CH_3OH can

reach 94–96% on the sample CuO-Cu_2O nanorod. Under continuous illumination, the photoexcited electrons can transfer from Cu_2O to CuO, or directly to CO_2 adsorbed on the surface of the catalyst, improving the photoelectrochemical performance (Figure 9b). Later, Li et al. prepared Fe_2O_3 nanotubes modified with double-layer Cu_2O spheres (Cu_2O/Fe_2O_3 NTs) by electrodeposition method for PEC CO_2RR (Figure 9c) [89]. Cu_2O/Fe_2O_3 NTs-30 showed a three-layer structure: the bottom layer was Fe_2O_3 nanotubes, the middle layer was Cu_2O spheres of 200–500 nm, and the top layer was Cu_2O spheres with a larger diameter (Figure 9d,e). This novel three-layer structure successfully converted CO_2 to CH_3OH in 6 h and the FE of CH_3OH was as high as 93% at −1.3 V vs. SCE, which was higher than Cu_2O/Fe and Fe_2O_3 NTs (Figure 9f). The efficient conversion of CO_2 into CH_3OH is mainly because the novel three-layer structure has a conduction band position suitable for CO_2 reduction and the synergy between PC and EC can promote electron transfer (Figure 9g). Further focus on the effect of Fe:Cu ratio on the product distribution over Cu_2O/Fe_2O_3 will be more helpful in exploring its reaction kinetics and product selectivity.

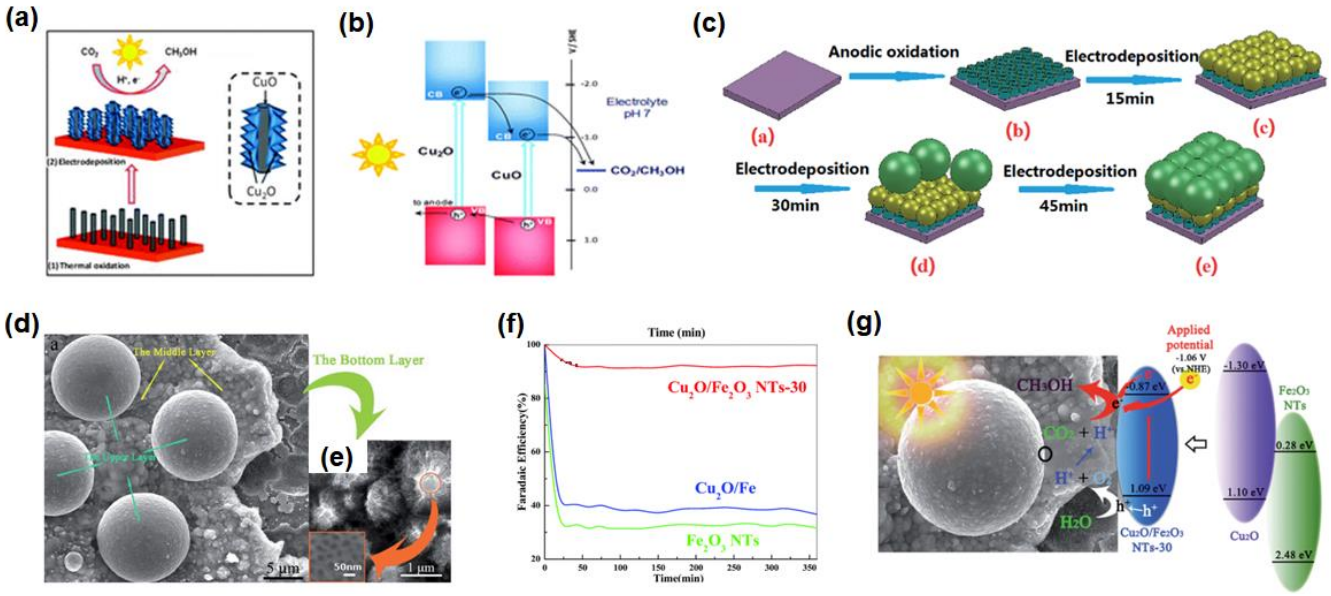


Figure 9. (**a**) Schematic diagram of CuO/Cu_2O nanorod synthesis and the CO_2RR; (**b**) energy band diagram and electron transfer route of CuO/Cu_2O nanorod array for the synthesis of CH_3OH. Adapted with permission from Ref. [64]. Copyright 2013, Royal Society of Chemistry. (**c**) Growth mechanism of Cu_2O/Fe_2O_3NTs-30 composite; (**d**,**e**) SEM of Cu_2O/Fe_2O_3 NTs-30; (**f**) FE of CH_3OH on Cu_2O/Fe_2O_3 NTs-30, Cu_2O/Fe, and Fe_2O_3 NTs; (**g**) mechanism of the PEC CO_2RR on Cu_2O/Fe_2O_3 NTs-30 nanotubes (30: electrodeposition times). Adapted with permission from Ref. [89]. Copyright 2014, Royal Society of Chemistry.

Recently, Kang et al. [90] prepared a hierarchically structured photocathode material Cu_2O/TiO_2 by controlling the synthesis temperature, atmosphere and pressure (Figure 10a). The single-phase Cu_2O could be obtained by analyzing the chemical potential and accurately calculating the Gibbs free energy of CuO, Cu_2O, and Cu (Figure 10b,c). In PEC CO_2RR, TiO_2 can protect Cu_2O from corrosion, but the photogenerated electrons, on the CB of Cu_2O, directly participate in CO_2RR through the TiO_2 layer (Figure 10d,e). Interestingly, when the thickness of the TiO_2 layer is higher than 5 nm, TiO_2 and Cu_2O mainly form a p-n heterojunction and the photogenerated electrons on Cu_2O can transfer to TiO_2. Therefore, whether TiO_2 participates in the transfer of electrons mainly depends on its thickness. Through the ingenious design of fewer than 5 nm thick TiO_2 and pure phase cuprous oxide composite material, the stability and photoactivity have been greatly improved compared with pure Cu_2O or only deposition TiO_2 on the pure Cu_2O but not thermodynamically programmed calcination (Figure 10f). The selectivity of CH_3OH exceeds 90%

on the Cu_2O/TiO_2 with 5 nm TiO_2 layers (Figure 10g), effectively demonstrating that the products based on Cu-based photocathodes achieve high selectivity. Nevertheless, this synthesis method is relatively complex, which is not conducive to large-scale promotion.

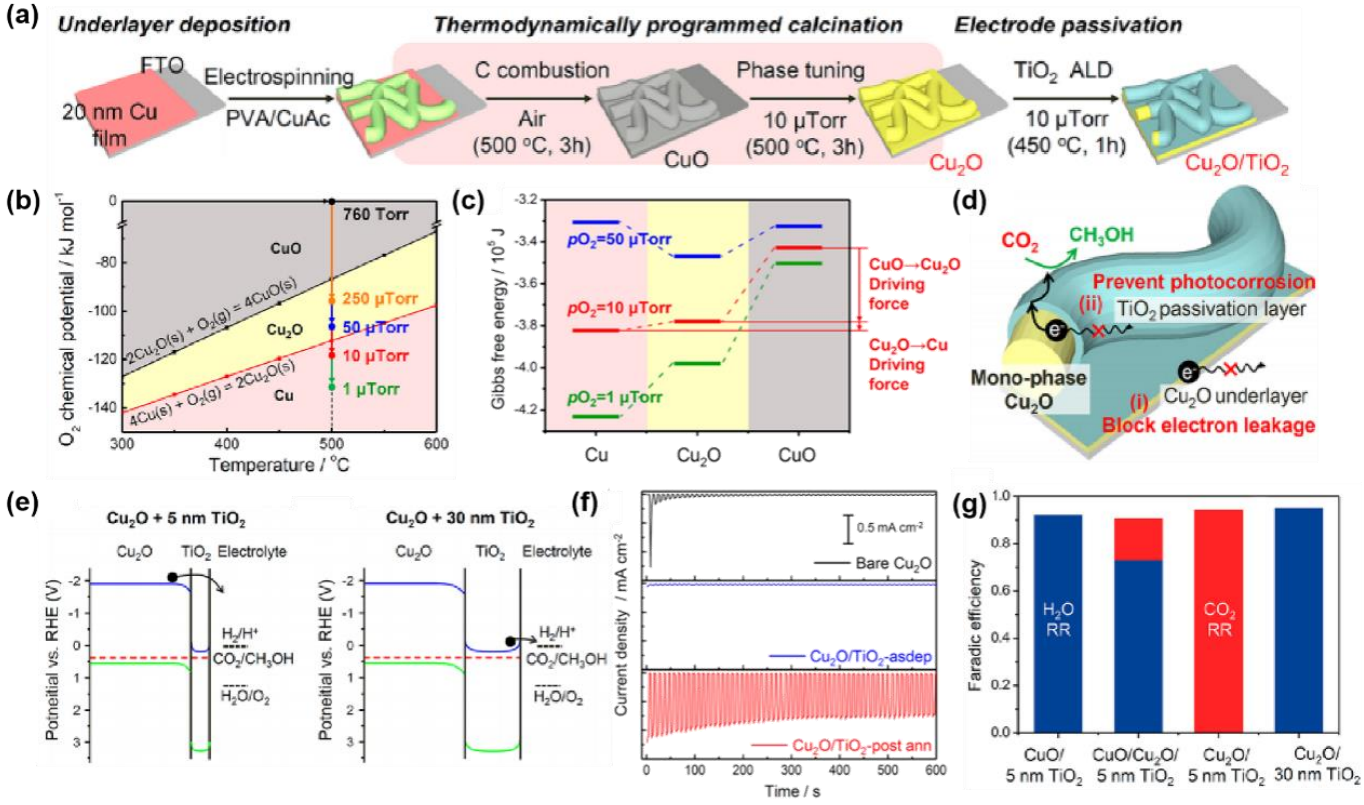


Figure 10. (**a**) The preparation process of hierarchically structured Cu_2O/TiO_2 photocathode; (**b**) diagram of the chemical potential of oxygen at different temperatures; (**c**) calculation of the Gibbs free energy of O_2 at different pressures; (**d**) schematic of the hierarchical structure of Cu_2O/TiO_2; (**e**) band diagram of the Cu_2O/TiO_2 system with different thickness of the TiO_2 passivation layer (blue line: CB, green line: VB, red dashed line: forbidden ban); (**f**) the effect of TiO_2 passivation and the post-annealing process on photostability; (**g**) FE of CO_2RR for different samples. Adapted with permission from Ref. [90]. Copyright 2018, American Chemical Society.

4.3.6. g-C_3N_4-Based Photoelectrodes

g-C_3N_4 is a polymer semiconductor with a bandwidth of 2.7 eV, which has high chemical stability under visible light irradiation, high reduction capacity, and sensitivity to visible light [91,92]. Recently, Nobuhiro Sagara et al. [57] prepared B-doped g-C_3N_4 (BCN_x) for PEC CO_2RR to CH_3CH_2OH. Although g-C_3N_4 is an n-type semiconductor, B-doped g-C_3N_4 is a proven p-type semiconductor. Compared with the pure g-C_3N_4, the potentials of the CB and VB of the sample BCN_x are significantly increased, but the potential of the CB is still sufficient to reduce the CO_2 (Figure 11a). It has been found that the photocurrent response of the sample BCN_x could be improved after doping B (Figure 11b). Moreover, the photocurrent response on the different co-catalyst (Au, Ag, Rh)-loaded $BCN_{3.0}$ could be further improved (Figure 11c). Rh or Au-loaded $BCN_{3.0}$ show a higher number of products than $BCN_{3.0}$ (Figure 11d), but the FEs of CH_3CH_2OH on Rh-loaded $BCN_{3.0}$ (36%) and Au-loaded $BCN_{3.0}$ (47%) are lower than Ag-loaded, B-doped $BCN_{3.0}$ (73%) and $BCN_{3.0}$ (78%).

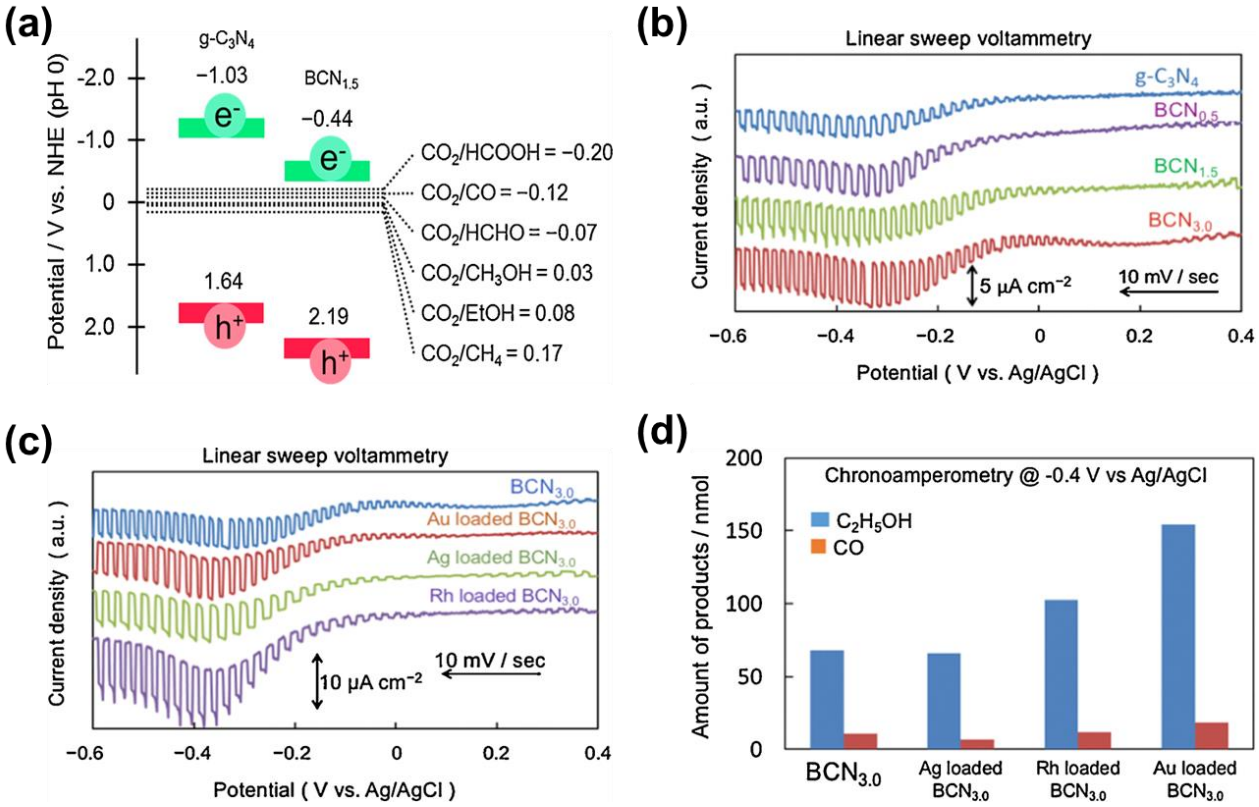


Figure 11. (**a**) Band potential diagram for g-C_3N_4 and $BCN_{1.5}$ together with the thermodynamic potentials for CO_2 reduction to various reduction products vs. NHE at pH 0; (**b**) linear sweep voltammetry of the g-C_3N_4 and BCN_x electrodes; (**c**) linear sweep voltammetry of the $BCN_{3.0}$ electrodes loaded with or not loaded with co-catalysts; (**d**) product analyses of photoelectrochemical reduction of CO_2 over co-catalyst loaded $BCN_{3.0}$ electrodes. Adapted with permission from Ref. [57]. Copyright 2016, Elsevier Ltd.

The composite g-C_3N_4 and ZnTe, as a photocathode, can form a type II heterojunction and convert CO_2 to CH_3CH_2OH [93]. Through the analysis of the UV-vis absorption spectra, the composite g-C_3N_4/ZnTe presents similar visible light adsorption performance and bandwidth to pure ZnTe (Figure 12a). According to PL spectra, it has been found that the peak intensity of the sample g-C_3N_4/ZnTe is significantly lower than ZnTe, indicating that the g-C_3N_4/ZnTe has a lower electron-hole recombination rate (Figure 12b). The yield of CH_3CH_2OH on the heterojunction g-C_3N_4/ZnTe is 17.1 μmol $cm^{-2}{\cdot}h^{-1}$ at −1.1 V vs. Ag/AgCl, and the competitive hydrogen evolution is efficiently suppressed (Figure 12c), which is ascribed to the ZnTe with high CO_2 adsorption capacity, and g-C_3N_4 rich in pyridine N contributes to C-C coupling. Moreover, a pipeline mechanism has been proposed to explain the PEC CO_2RR process (Figure 12d), consisting of three steps: the adsorption and activation of CO_2, the formation of CO intermediate, and the adsorption of CO intermediate on pyridine N. DFT theoretical calculations indicated that pyridine N sites were very important for the adsorption of intermediates and the formation of ethanol. The results of the studies show that polymer semiconductors, and metal loads used for the construction of heterojunctions, are also effective for PEC CO_2RR. It is expected that advanced film preparation methods will further improve the film quality of g-C_3N_4/ZnTe photocathodes to achieve effective charge separation, which will enhance the activity of PEC CH_3CH_2OH production.

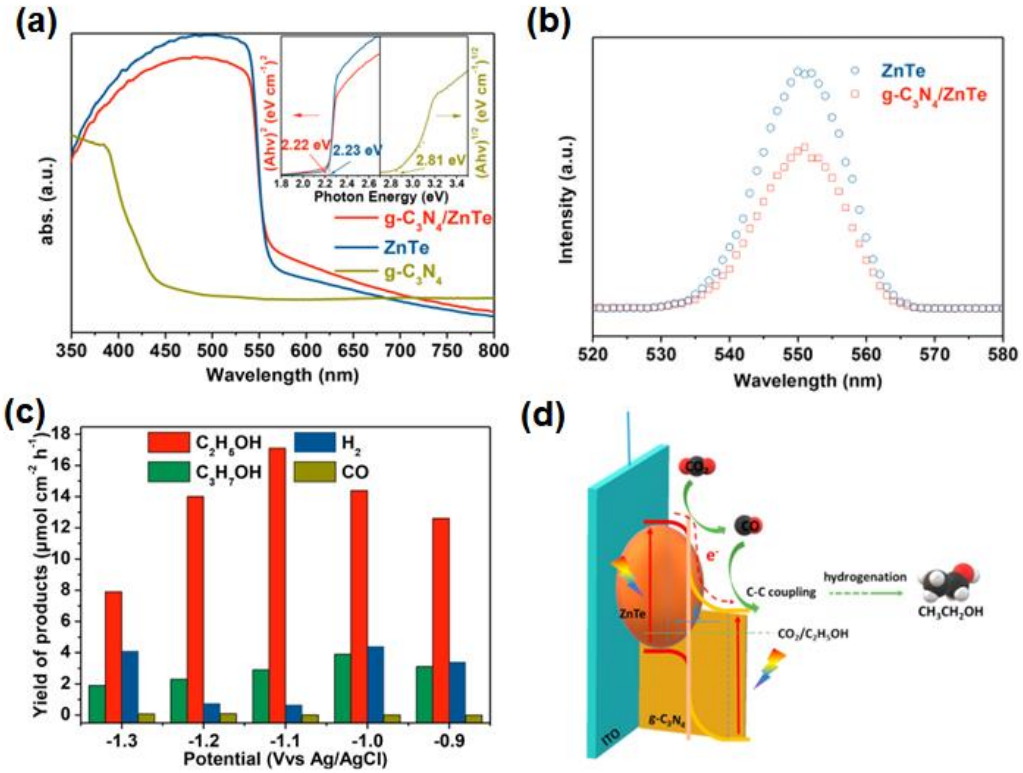


Figure 12. (**a**) UV–vis diffuse reflectance spectra of three photocathodes g-C_3N_4/ZnTe, g-C_3N_4 and ZnTe; (**b**) PL spectra for g-C_3N_4/ZnTe and ZnTe; (**c**) products of g-C_3N_4/ZnTe for PEC CO_2RR at different applied potentials; (**d**) schematic diagram of formed heterojunction and the charge separation process. Adapted with permission from Ref. [93]. Copyright 2019, Elsevier Ltd.

4.3.7. Titanium (Ti)-Based Photoelectrodes

The main structures of TiO_2 are rutile and anatase, with band gaps of 3.2 eV and 3.0 eV, respectively [94]. TiO_2, as the most popular semiconductor, is very stable under ultraviolet light and can be used as a photoanode or a photocathode. However, TiO_2 shows a weak adsorption performance in the visible range. Cardoso et al. [95] reported that Ti/TiO_2 nanotubes (TiO_2NT) modified ZIF-8 as a photocathode for the PEC CO_2RR (Figure 13a). It has been found that pure ZIF-8 absorbs very little visible light, while the Ti/TiO_2NT-ZIF-8 shows an enhanced visible light absorption performance and reduced bandwidth, compared with Ti/TiO_2NT, implying an interaction between nanotubes of Ti/TiO_2NT and ZIF-8 (Figure 13b,c). In the PEC CO_2RR, the selectivity to CH_3CH_2OH of the sample Ti/TiO_2NT-ZIF-8 increased significantly, and its conversion rate increased by nearly 430 times in 1 h at −0.7 V vs. Ag/AgCl (Figure 13d). Compared with PC CO_2RR, the conversion of CO_2 significantly improved in the PEC CO_2RR, owing to the synergy of light and electricity (Figure 13e). Moreover, ascorbic acid (AA) as a sacrificial agent was also studied in the PEC CO_2RR [96]. Sacrificial agents, as donors of electrons, can promote the conversion of CO_2 and increase CH_3CH_2OH conversion, and the FE of CH_3CH_2OH reached 86% on the sample Ti/TiO_2NT and ZIF-8 in the presence of AA (Figure 13f). The reduced N sites of imidazolate groups in ZIF-8 can enhance the adsorption of CO_2 and form carbamate to promote CO_2 conversion. Meanwhile, imidazole compounds can act as electron acceptors to enhance light absorption, and thus improve photocurrent response. Such a combination of titania with MOF materials shows great potential in PEC CO_2RR. Additionally, the results show that adding a sacrificial agent to the reaction is also an effective way to improve the selectivity of the product.

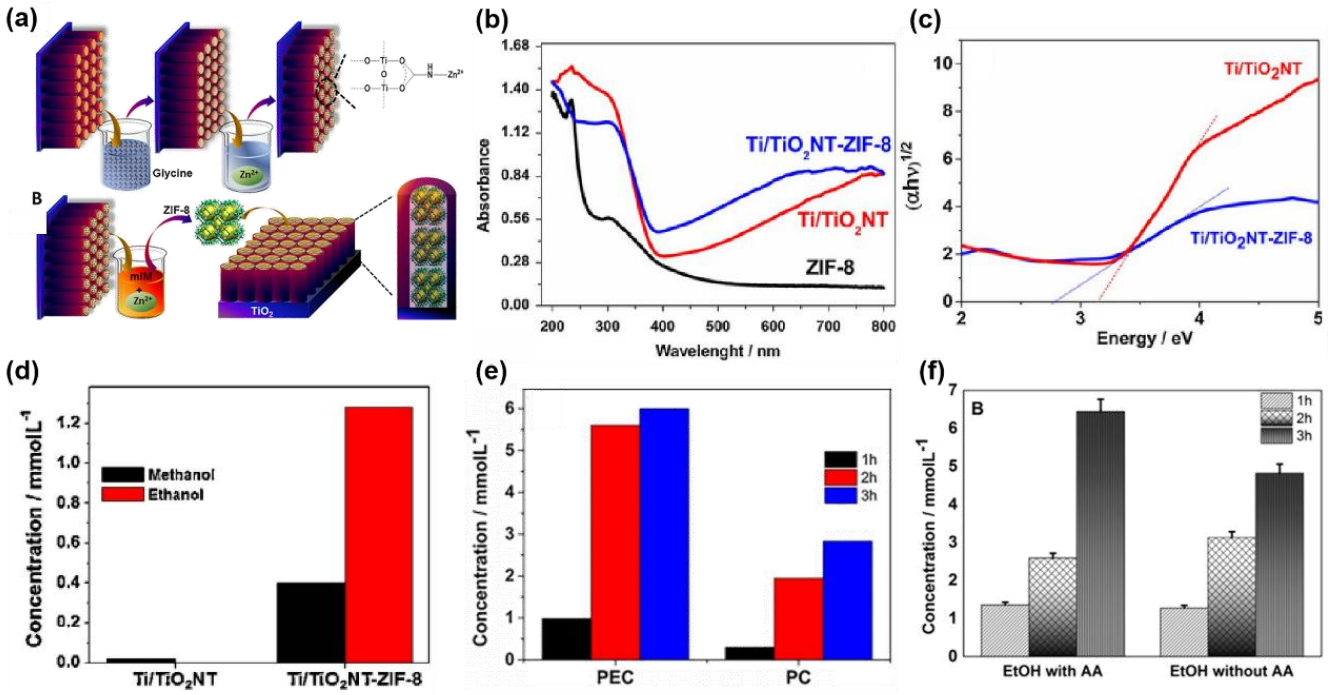


Figure 13. (**a**) Synthetic diagram of Ti/TiO_2NT-ZIF-8; (**b**) UV–vis absorption spectra of ZIF-8, TiO_2NT, and TiO_2NT-ZIF-8; (**c**) Tauc plot of Ti/TiO_2NT and Ti/TiO_2NT-ZIF-8; (**d**) concentrations of methanol and ethanol generated in the PEC processes at −0.7 V vs. Ag/AgCl, in 0.1 mol L^{-1} Na_2SO_4 (pH 4.5), using the Ti/TiO_2NT and Ti/TiO_2NT-ZIF-8 electrodes for 1 h; (**e**) the concentration of ethanol generated by using sample Ti/TiO_2NT-ZIF-8 in the PEC and PC CO_2RR. Adapted with permission from Ref. [95]. Copyright 2017, Elsevier B.V. (**f**) The concentration of ethanol on the sample Ti/TiO_2NT-ZIF-8 with and without ascorbic acid (AA) in the PEC CO_2RR. Adapted with permission from Ref. [96]. Copyright 2019, Elsevier B.V.

The products and performance of different representative catalysts mentioned above were summarized in Table 2.

Table 2. Summary of products and PEC CO_2 reduction performance of different representative photocathodes.

Category	Product	Catalyst	Current Density	FE (%)	Ref.
Zi-based	CO	ZnTe/ZnO (ZOZT)	−7.89 mA·cm^{-2} (at −0.7 V vs. RHE)	7.2	[62]
	CO	ZOZT-Au	−15.97 mA·cm^{-2} (at −0.7 V vs. RHE)	58.0	[62]
Co-based	HCOOH	Cu-Co_3O_4 NTs	−0.122 mA·cm^{-2} (at −0.9 V vs. NHE)	-	[75]
	HCOOH	Ru(bpy)$_2$dppz-Co_3O_4/CA	8.1 mA·cm^{-2} (at −0.6 V vs. NHE)	86	[72]
	HCOOH	ZIF9-Co_3O_4	1 mA·cm^{-2} (at −0.9 V vs. SCE)	70.5	[76]
Si-based	CO	Si-w/RA Au	−2.94 mA·cm^{-2} (at −0.6 V vs. RHE)	96	[77]
	HCOOH	*p*-Si/Sn	~−1 mA·cm^{-2} (at −0.6 V vs. RHE)	88.4	[79]
	CO	Cu-ZnO/GaN/n^+-*p* Si	~−2 mA·cm^{-2} (at +0.07 V vs. RHE)	70	[80]

Table 2. *Cont.*

Category	Product	Catalyst	Current Density	FE (%)	Ref.
Fe-based	HCOOH	$CuFeO_2$/Mg	−1 mA·cm^{-2} (at −0.9 V vs. SCE)	10	[56]
	HCOOH	$CuFeO_2$/CuO	−0.2 mA·cm^{-2} (at +0.9 V vs. RHE)	90	[65]
Cu-based	CH_3OH	CuO-Cu_2O nanorod	0.25 mA·cm^{-2} (at −0.2 V vs. SHE)	94–96	[64]
	CH_3OH	Cu_2O/Fe_2O_3 NTs	~15 μA·cm^{-2} (at −0.6 V vs. SHE)	93	[89]
g-C_3N_4-based	CH_3CH_2OH	$BCN_{3.0}$	~5 μA·cm^{-2} (at −0.4 V vs. Ag/AgCl)	78	[57]
	CH_3CH_2OH	$BCN_{3.0}$/Ag	~10 μA·cm^{-2} (at −0.4 V vs. Ag/AgCl)	73	[57]
Ti-based	CH_3CH_2OH	Ti/TiO_2 NT-ZIF-8	~−1.5 mA·cm^{-2} (at −0.7 V vs. Ag/AgCl)	86	[96]

5. Possible PEC CO_2RR Mechanisms

CO_2 has stable chemical properties and low reactivity; thus, high energy is required to realize the conversion of $CO_2^{\cdot}$. Moreover, CO_2RR is also a complex process involving the coupling of many protons and the electron transfer processes. Using different catalysts and controlling the reaction conditions in the PEC CO_2RR, different products could be generated. Generally, the conversion of CO_2 to C_1 and C_2 products is easier than other complex hydrocarbon products. Up to now, though the mechanism of CO_2RR is not particularly clear, many possible reaction pathways have been proposed [21].

Table 3 provides the possible half-reactions of electrochemical CO_2 reduction and the electrochemical potential of thermodynamically stable CO_2 molecules into C_1, C_2 and C_3 hydrocarbon molecules. Wherein, the CO_2 molecule combines with an electron to form anion radical intermediate $CO_2^{\cdot -}$, which is generally regarded as the rate-limiting step, since this step needs to overcome a large redox potential, which is much higher than that required by other processes.

Table 3. The CO_2 reduction potential in aqueous solutions for the production of different hydrocarbon fuels [97].

Possible Half-Reaction Electrochemical CO_2 Reduction	Electrode Potentials (V vs. SHE) at pH 7
CO_2 (g) + e^- → *COO^-	−1.90
CO_2 (g) + 2H^+ + 2e^- → HCOOH	−0.61
CO_2 (g) + 2H^+ + 2e^- → CO (g) + H_2O (l)	−0.53
CO_2 (g) + 4H^+ + 2e^- → HCHO (l) + H_2O (l)	−0.48
CO_2 (g) + 6H^+ + 6e^- → CH_3OH (l) + H_2O (l)	−0.38
CO_2 (g) + 8H^+ + 8e^- → CH_4 (g) + 2H_2O (l)	−0.24
CO_2 (g) + 12H^+ + 12e^- → C_2H_4 (g) + 4H_2O (l)	0.06
2CO_2 (g) + 12H^+ + 12e^- → CH_3CH_2OH (l) + 3H_2O (l)	0.08
2CO_2(g) + 14H^+ + 14e^- → CH_3CH_3 (g) + 4H_2O (l)	−0.27

At present, researchers have explored CO_2 reduction pathways using elemental catalysts, especially metals, and proposed possible mechanisms of CO_2 reduction in the aqueous solution, as shown in Figure 14 [97]. In the activation process, the straight CO_2 molecule can bend as it gains electrons. Additionally, different catalysts have different adsorption strengths for the intermediate and can stabilize different intermediates, thus producing various products, which is essential for the efficient conversion of CO_2.

The main products of CO_2RR on the transition metals are CO and HCOOH, and the binding energy of the first intermediate and the catalyst influences the final product. When the intermediate $CO_2^{\cdot -}$ is weakly adsorbed on the catalyst surface, HCOOH or $HCOO^-$ is the main product, and the metal catalysts applied in this reaction are mainly Sn, In, Hg, Pb, etc.

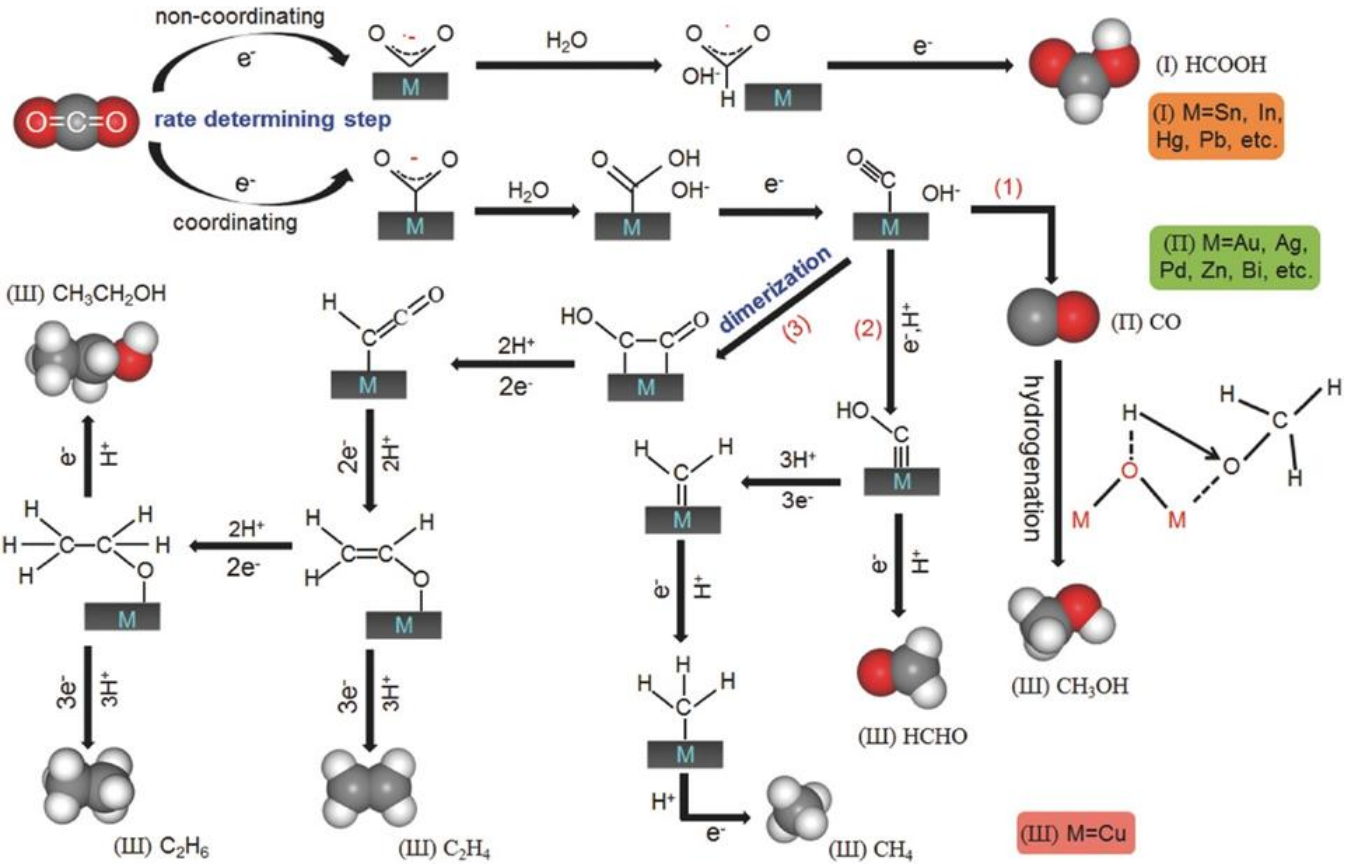


Figure 14. Schematic mechanism of CO_2 reduction on metal electrodes in aqueous solution. Reprinted with permission from Ref. [97]. Copyright 2018, Wiley.

Furthermore, some researchers also believe that the intermediate $CO_2^{\cdot -}$, that produces HCOOH or $HCOO^-$, may also bind to the catalyst by one or two oxygen atoms, but the source of hydrogen for this mechanism is unclear. It is generally believed that hydrogen can include at least two sources: (1) a metallic hydrogen bond; and (2) hydrogen protons in solution (Figure 15a–c) [98]. With regard to the metal catalysts Au, Ag, and Zn, etc., they can be closely combined with $CO_2^{\cdot -}$ and *COOH, but it is difficult to combine with the generated *CO intermediate, thus the reduction product is mainly CO. Based on previous research, it is known that Cu is a special metal, which can produce more complex carbon products. Firstly, the *CO intermediate is generated, then the formation of subsequent production products can be roughly divided into three pathways: (1) the combination of electrons and hydrogen protons to form the CO and H_2O; (2) the conversion of intermediate *CO to *CHO or *COH and the formation of CH_3OH or CH_4; (3) dimerizing itself to obtain different products, such as CH_3CH_2OH, HCHO, etc. by getting different numbers of electrons and protons (Figures 14 and 15b).

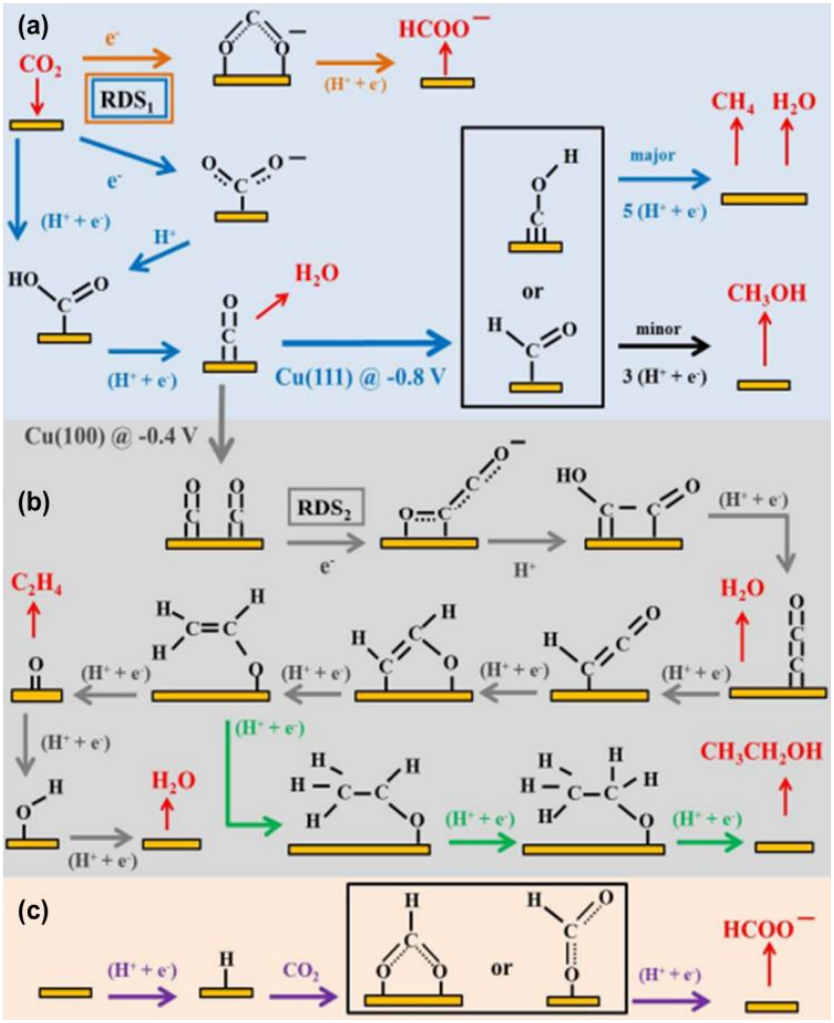


Figure 15. (**a**–**c**) Schematic mechanisms of CO_2 reduction on Cu electrodes in aqueous solution. Adapted with permission from Ref. [98]. Copyright 2015, American Chemical Society.

In addition, another mechanism is to avoid the formation of $CO_2^{\bullet -}$ intermediate by proton-coupled electron transfer (PCET) [99]. The activation barrier caused by high recombination energy and unstable intermediates is avoided by the transfer of a proton with an electron, but the proton concentration, pH, and temperature and other synthesis conditions have a greater impact on the PECT process [100,101].

In summary, there are still many unclear factors and processes in the PEC CO_2RR, and the research on its catalytic mechanism is still in its infancy. Therefore, we need to further explore the related mechanisms of CO_2RR, based on the experiment dates, advanced characteristic techniques, and DFT calculations.

6. Conclusions, Remarks, and Outlook

In the face of the global energy crisis and increasingly serious environmental issues, the reduction of CO_2 and the utilization of natural resources (light) have attracted significant attention. The current research, including the design of photocathodes to achieve effective CO_2 reduction by doping metal and non-metal; construction of heterojunctions such as Z-type heterojunctions, type II heterojunctions and even p-p type heterojunctions; as well as modification of co-catalysts, etc., has made great progress. Nevertheless, there are still great challenges in the practical applications; for example, the problems of low photocurrent density, low FE of reduction products, poor yield of products, and serious photo-corrosion of photocathode materials, etc.

The design of photocathode materials is crucial to the PEC CO_2RR process. How to improve the light absorption of the designed photocathode material, as well as how to promote the separation of charge carriers and improve the selectivity of the product, etc., will be the emphases of the research. To this end, the following issues should also be taken into consideration:

Firstly, it is crucial to develop a new p-type semiconductor photocathode material with good stability, ultra-visible light adsorption, and CO_2 conversion performance. Although some p-type semiconductor materials have been developed as photocathodes to achieve the application of PEC CO_2RR, most of them have serious issues such as photo-corrosion and the complexity of reduction products. Therefore, the developed new p-type photocathode material should have photo corrosion resistance and good selectivity for CO_2 reduction products. However, the development of new photocathode materials is relatively difficult and requires a long-term process, which requires deeper theoretical foundations and the assistance of DFT calculations.

Secondly, a highly efficient catalyst can be designed by reasonably optimizing the structure and composition, which is currently one of the most universally applicable measures to achieve highly efficient CO_2 reduction. For example, the combination of photocatalysts with good light absorption and electrocatalysts with super selectivity in CO_2RR not only preserves the advantages of each component but also regulates the selectivity of the product. More importantly, by loading co-catalysts, visible light can be effectively utilized and photogenerated electrons can be effectively separated. In addition, metals have stronger conductivity, and metal co-catalysts can thus increase current density, making them closer to industrial applications. At the same time, in the design of photocathode materials, combining semiconductor materials with appropriate conduction band positions is also an effective mean of promoting CO_2 reduction.

Thirdly, improving or optimizing the catalyst preparation process is also an effective way to improve its performance, such as surface coating, surface modification, or a combination of surface technology. Different preparation processes can expose different crystal planes or generate different surface states and configurations, which are conducive to the adsorption of CO_2 and the desorption of intermediates and products, improving light utilization efficiency, and enhancing the activity and stability of catalytic reactions. Moreover, it is also crucial to control and regulate the contact interface of photocathode materials. Additionally, the contact interface generally serves as a barrier for electron transfer, so precise control of the contact interface can effectively promote the separation of photo-generated charge carriers. For example, more active sites or defects can be exposed at the interface contact with electrolytes, to promote CO_2 activation.

Last but not least, it is necessary to further strengthen the exploration of CO_2 reduction mechanisms. A better understanding of the mechanism helps to design the structure of the target catalyst and achieve effective CO_2 conversion, especially through theoretical calculations, to strengthen the study of the internal relationship between kinetics and thermodynamics.

Overall, PEC CO_2RR is a promising approach for addressing fossil fuel depletion and mitigating greenhouse effects. Based on the existing technologies, combined with the development of new materials, reasonable design of catalyst structure and components, and optimization or improvement of preparation methods, it is expected to achieve more efficient CO_2 conversion.

Author Contributions: K.X. and Q.Z. have equally contributed to the manuscript. Investigation, K.X., Q.Z., M.Z. and X.Z.; writing—original draft preparation, K.X. and Q.Z.; writing, review and editing, K.X., X.Z. and H.C.; supervision, H.C.; project administration, H.C.; funding acquisition, H.C. All authors have read and agreed to the published version of the manuscript.

Funding: This review was funded by the National Natural Science Foundation of China (51961165107), and the project of the Shanghai Science and Technology Commission (19520761000).

Conflicts of Interest: The authors declare no conflict of interest.

Abbreviations

PEC	Photoelectrochemical
CO_2RR	Carbon dioxide reduction reaction
PC	Photocatalysis
EC	lectrochemical
FE	Faraday efficiency
STF	Solar-to-fuel efficiency
IPCE	Incident photon-to-current efficiency
APCE	Absorbed photon-current conversion efficiency
TON	Turnover number
TOF	Turnover frequency
RHE	Reversible hydrogen electrode
NHE	Normal hydrogen electrode
SCE	Saturated calomel electrode
CB	Conduction band
VB	Valence band
AA	Ascorbic acid
PCET	Proton-coupled electron transfer

References

1. Chen, Z.; Zhang, G.; Chen, H.; Prakash, J.; Zheng, Y.; Sun, S. Multi-metallic catalysts for the electroreduction of carbon dioxide: Recent advances and perspectives. *Renew. Sustain. Energy Rev.* **2022**, *155*, 111922. [CrossRef]
2. Jinmo, K.; Woong, C.; Woo, P.J.; Cheonghee, K.; Minjun, K.; Hyunjoon, S. Branched Copper Oxide Nanoparticles Induce Highly Selective Ethylene Production by Electrochemical Carbon Dioxide Reduction. *J. Am. Chem. Soc.* **2019**, *141*, 6986–6994.
3. Michele, A. Catalysis for the valorization of exhaust carbon: From CO_2 to chemicals, materials, and fuels. Technological use of CO_2. *Chem. Rev.* **2014**, *3*, 1709–1742.
4. Liu, Y.; Yang, Y.; Sun, Q.; Wang, Z.; Huang, B.; Dai, Y.; Qin, X.; Zhang, X. Chemical Adsorption Enhanced CO_2 Capture and Photoreduction over a Copper Porphyrin Based Metal Organic Framework. *ACS Appl. Mater. Interfaces* **2013**, *5*, 7654–7658. [CrossRef] [PubMed]
5. Zhao, K.; Liu, Y.; Quan, X.; Chen, S.; Yu, H. CO_2 Electroreduction at Low Overpotential on Oxide-Derived Cu/Carbons Fabricated from Metal Organic Framework. *ACS Appl. Mater. Interfaces* **2017**, *9*, 5302–5311. [CrossRef] [PubMed]
6. Diau, E.W.-G. Next-Generation Solar Cells and Conversion of Solar Energy. *ACS Energy Lett.* **2017**, *2*, 334–335. [CrossRef]
7. Feng, X.; Zou, H.; Zheng, R.; Wei, W.; Wang, R.; Zou, W.; Lim, G.; Hong, J.; Duan, L.; Chen, H. Bi_2O_3/BiO_2 Nanoheterojunction for Highly Efficient Electrocatalytic CO_2 Reduction to Formate. *Nano Lett.* **2022**, *22*, 1656–1664. [CrossRef]
8. Yoon, T.P.; Ischay, M.A.; Du, J. Visible light photocatalysis as a greener approach to photochemical synthesis. *Nat. Chem.* **2010**, *2*, 527–532. [CrossRef]
9. Kondratenko, E.V.; Mul, G.; Baltrusaitis, J.; Larrazábal, G.O.; Pérez-Ramírez, J. Status and perspectives of CO_2 conversion into fuels and chemicals by catalytic, photocatalytic and electrocatalytic processes. *Energy Environ. Sci.* **2013**, *6*, 3112–3135. [CrossRef]
10. Gao, J.; Bahmanpour, A.; Kröcher, O.; Zakeeruddin, S.M.; Ren, D.; Grätzel, M. Electrochemical synthesis of propylene from carbon dioxide on copper nanocrystals. *Nat. Chem.* **2023**, *15*, 705–713. [CrossRef]
11. Li, H.; Yue, X.; Che, J.; Xiao, Z.; Yu, X.; Sun, F.; Xue, C.; Xiang, J. High Performance 3D Self-Supporting Cu-Bi Aerogels for Electrocatalytic Reduction of CO_2 to Formate. *ChemSusChem* **2022**, *15*, e202200226. [PubMed]
12. Kecsenovity, E.; Endrődi, B.; Pápa, Z.; Hernádi, K.; Rajeshwar, K.; Janáky, C. Decoration of ultra-long carbon nanotubes with Cu_2O nanocrystals: A hybrid platform for enhanced photoelectrochemical CO_2 reduction. *J. Mater. Chem. A* **2016**, *4*, 3139–3147. [CrossRef]
13. Sivula, K.; Roel, V.D.K. Semiconducting materials for photoelectrochemical energy conversion. *Nat. Rev. Mater.* **2016**, *1*, 15010. [CrossRef]
14. Albero, J.; Peng, Y.; García, H. Photocatalytic CO_2 Reduction to C2+ Products. *ACS Catal.* **2020**, *10*, 5734–5749. [CrossRef]
15. Kočí, K.; Van, H.D.; Edelmannová, M.; Reli, M.; Wu, J.C. Photocatalytic reduction of CO_2 using Pt/C3N4 photocatalyts. *Appl. Surf. Sci.* **2020**, *503*, 144426. [CrossRef]
16. Lee, W.; Kim, Y.E.; Youn, M.H.; Jeong, S.K.; Park, K.T. Catholyte-Free Electrocatalytic CO_2 Reduction to Formate. *Angew. Chem. Int. Ed.* **2018**, *57*, 6883–6887. [CrossRef] [PubMed]
17. Mezzavilla, S.; Horch, S.; Stephens, I.E.L.; Seger, B.; Chorkendorff, I. Structure Sensitivity in the Electrocatalytic Reduction of CO_2 with Gold Catalysts. *Angew. Chem. Int. Ed.* **2019**, *58*, 3774–3778. [CrossRef]
18. Roger, I.; Shipman, M.A.; Symes, M.D. Earth-abundant catalysts for electrochemical and photoelectrochemical water splitting. *Nat. Rev. Chem.* **2017**, *1*, 3. [CrossRef]
19. Zhang, N.; Long, R.; Gao, C.; Xiong, Y. Recent progress on advanced design for photoelectrochemical reduction of CO_2 to fuels. *Sci. China Mater.* **2018**, *61*, 771–805. [CrossRef]

20. Zhang, Q.; Zhou, X.; Kuang, Z.; Xue, Y.; Li, C.; Zhu, M.; Mou, C.; Chen, H. A Bismuth Species-Decorated ZnO/p-Si Photocathode for High Selectivity of Formate in CO_2 Photoelectrochemical Reduction. *ACS Sustain. Chem. Eng.* **2022**, *10*, 2380–2387. [CrossRef]
21. White, J.L.; Baruch, M.F.; Pander, J.E., III; Hu, Y.; Fortmeyer, I.C.; Park, J.E.; Zhang, T.; Liao, K.; Gu, J.; Yan, Y.; et al. Light-Driven Heterogeneous Reduction of Carbon Dioxide: Photocatalysts and Photoelectrodes. *Chem. Rev.* **2015**, *115*, 12888–12935. [CrossRef] [PubMed]
22. Xiaoxia, C.; Tuo, W.; Piaoping, Y.; Gong, Z.; Gong, J. The Development of Cocatalysts for Photoelectrochemical CO_2 Reduction. *Adv. Mater.* **2019**, *31*, 1804710.
23. Yuan, J. Photoelectrochemical Reduction of Carbon Dioxide to Ethanol at Cu_2O Foam Cathode. *Int. J. Electrochem. Sci.* **2017**, *12*, 8288–8294. [CrossRef]
24. Schreier, M.; Luo, J.; Gao, P.; Moehl, T.; Mayer, M.T.; Grätzel, M. Covalent Immobilization of a Molecular Catalyst on Cu_2O Photocathodes for CO_2 Reduction. *J. Am. Chem. Soc.* **2016**, *138*, 1938–1946. [CrossRef]
25. Chertkova, V.P.; Iskortseva, A.N.; Pazhetnov, E.M.; Arkharova, N.A.; Ryazantsev, S.V.; Levin, E.E.; Nikitina, V.A. Evaluation of the Efficiency of Photoelectrochemical Activity Enhancement for the Nanostructured $LaFeO_3$ Photocathode by Surface Passivation and Co-Catalyst Deposition. *Nanomaterials* **2022**, *12*, 4327. [CrossRef]
26. Barton, E.E.; Rampulla, D.M.; Bocarsly, A.B. Selective Solar-Driven Reduction of CO_2 to Methanol Using a Catalyzed p-GaP Based Photoelectrochemical Cell. *J. Am. Chem. Soc.* **2008**, *130*, 6342–6344. [CrossRef]
27. Flaisher, H.; Tenne, R.; Halmann, M. Photoelectrochemical reduction of carbon dioxide in aqueous solutions on p-GaP electrodes: An a.c. impedance study with phase-sensitive detection. *J. Electroanal. Chem.* **1996**, *402*, 97–105. [CrossRef]
28. Noh, S.; Shin, J.; Yu, Y.-T.; Ryu, M.-Y.; Kim, J.S. Manipulation of Photoelectrochemical Water Splitting by Controlling Direction of Carrier Movement Using InGaN/GaN Hetero-Structure Nanowires. *Nanomaterials* **2023**, *13*, 358. [CrossRef]
29. Kobayashi, K.; Lou, S.N.; Takatsuji, Y.; Haruyama, T.; Shimizu, Y.; Ohno, T. Photoelectrochemical reduction of CO_2 using a TiO_2 photoanode and a gas diffusion electrode modified with a metal phthalocyanine catalyst. *Electrochim. Acta* **2020**, *338*, 135805. [CrossRef]
30. Xu, Y.; Jia, Y.; Zhang, Y.; Nie, R.; Zhu, Z.; Wang, J.; Jing, H. Photoelectrocatalytic reduction of CO_2 to methanol over the multi-functionalized TiO_2 photocathodes. *Appl. Catal. B Environ.* **2017**, *205*, 254–261. [CrossRef]
31. Hong, J.; Zhang, W.; Ren, J.; Xu, R. Photocatalytic reduction of CO_2: A brief review on product analysis and systematic methods. *Anal. Methods* **2013**, *5*, 1086–1097. [CrossRef]
32. Austin, N.; Ye, J.; Mpourmpakis, G. CO_2 activation on Cu-based Zr-decorated nanoparticles. *Catal. Sci. Technol.* **2017**, *7*, 2245–2251. [CrossRef]
33. Liu, W.; Zhai, P.; Li, A.; Wei, B.; Si, K.; Wei, Y.; Wang, X.; Zhu, G.; Chen, Q.; Gu, X.; et al. Electrochemical CO_2 reduction to ethylene by ultrathin CuO nanoplate arrays. *Nat. Commun.* **2022**, *13*, 1877. [CrossRef]
34. Ba, X.; Yan, L.-L.; Huang, S.; Yu, J.; Xia, X.-J.; Yu, Y. New Way for CO_2 Reduction under Visible Light by a Combination of a Cu Electrode and Semiconductor Thin Film: Cu_2O Conduction Type and Morphology Effect. *J. Phys. Chem. C* **2014**, *118*, 24467–24478. [CrossRef]
35. Wang, Y.; Liu, J.; Wang, Y.; Wang, Y.; Zheng, G. Efficient solar-driven electrocatalytic CO_2 reduction in a redox-medium-assisted system. *Nat. Commun.* **2018**, *9*, 5003. [CrossRef]
36. Kumar, B.; Atla, V.; Brian, J.P.; Kumari, S.; Nguyen, T.Q.; Sunkara, M.; Spurgeon, J.M. Reduced SnO_2 Porous Nanowires with a High Density of Grain Boundaries as Catalysts for Efficient Electrochemical CO_2-into-HCOOH Conversion. *Angew. Chem.* **2017**, *129*, 3699–3703. [CrossRef]
37. Hu, X.; Yang, H.; Guo, M.; Gao, M.; Zhang, E.; Tian, H.; Liang, Z.; Liu, X. Synthesis and Characterization of (Cu, S) Co-doped SnO_2 for Electrocatalytic Reduction of CO_2 to Formate at Low Overpotential. *Chemelectrochem* **2018**, *5*, 1330–1335. [CrossRef]
38. Kalamaras, E.; Maroto-Valer, M.M.; Shao, M.; Xuan, J.; Wang, H. Solar carbon fuel via photoelectrochemistry. *Catal. Today* **2018**, *317*, 56–75. [CrossRef]
39. Chen, Z.; Jaramillo, T.F.; Deutsch, T.G.; Kleiman-Shwarsctein, A.; Forman, A.J.; Gaillard, N.; Garland, R.; Takanabe, K.; Heske, C.; Sunkara, M.; et al. Accelerating materials development for photoelectrochemical hydrogen production: Standards for methods, definitions, and reporting protocols. *J. Mater. Res.* **2011**, *25*, 3–16. [CrossRef]
40. Pawar, A.U.; Kim, C.W.; Nguyen-Le, M.-T.; Kang, Y.S. General Review on the Components and Parameters of Photoelectrochemical System for CO_2 Reduction with in Situ Analysis. *ACS Sustain. Chem. Eng.* **2019**, *7*, 7431–7455. [CrossRef]
41. Lianos, P. Review of recent trends in photoelectrocatalytic conversion of solar energy to electricity and hydrogen. *Appl. Catal. B Environ.* **2017**, *210*, 235–254. [CrossRef]
42. Varghese, O.K.; Grimes, C.A. Appropriate strategies for determining the photoconversion efficiency of water photoelectrolysis cells: A review with examples using titania nanotube array photoanodes. *Sol. Energy Mater. Sol. Cells* **2008**, *92*, 374–384. [CrossRef]
43. Jiang, C.; Moniz, S.J.A.; Wang, A.; Zhang, T.; Tang, J. Photoelectrochemical devices for solar water splitting—Materials and challenges. *Chem. Soc. Rev.* **2017**, *46*, 4645–4660. [CrossRef] [PubMed]
44. Boudart, M. Turnover Rates in Heterogeneous Catalysis. *Chem. Rev.* **2002**, *95*, 661–666. [CrossRef]
45. Dunwell, M.; Luc, W.; Yan, Y.; Jiao, F.; Xu, B. Understanding Surface-Mediated Electrochemical Reactions: CO_2 Reduction and Beyond. *ACS Catal.* **2018**, *8*, 8121–8129. [CrossRef]
46. Arán-Ais, R.M.; Gao, D.; Cuenya, B.R. Structure- and Electrolyte-Sensitivity in CO_2 Electroreduction. *Acc. Chem. Res.* **2018**, *51*, 2906–2917. [CrossRef]

47. Li, C.; Zhou, X.; Zhang, Q.; Xue, Y.; Kuang, Z.; Zhao, H.; Mou, C.-Y.; Chen, H. Construction of Heterostructured Sn/TiO_2/Si Photocathode for Efficient Photoelectrochemical CO_2 Reduction. *ChemSusChem* **2022**, *15*, e202200188.
48. Xia, D.; Yu, H.; Xie, H.; Huang, P.; Menzel, R.; Titirici, M.M.; Chai, G. Recent progress of Bi-based electrocatalysts for electrocatalytic CO_2 reduction. *Nanoscale* **2022**, *14*, 7957–7973. [CrossRef]
49. Li, D.; Yang, K.; Lian, J.; Yan, J.; Liu, S. Powering the World with Solar Fuels from Photoelectrochemical CO_2 Reduction: Basic Principles and Recent Advances. *Adv. Energy Mater.* **2022**, *12*, 2201070. [CrossRef]
50. Ji, S.; Jiang, B.; Hao, H.; Chen, Y.; Dong, J.; Mao, Y.; Zhang, Z.; Gao, R.; Chen, W.; Zhang, R.; et al. Matching the kinetics of natural enzymes with a single-atom iron nanozyme. *Nat. Catal.* **2021**, *4*, 407–417. [CrossRef]
51. Ju, W.; Bagger, A.; Hao, G.-P.; Varela, A.S.; Sinev, I.; Bon, V.; Cuenya, B.R.; Kaskel, S.; Rossmeisl, J.; Strasser, P. Understanding activity and selectivity of metal-nitrogen-doped carbon catalysts for electrochemical reduction of CO_2. *Nat. Commun.* **2017**, *8*, 944. [CrossRef] [PubMed]
52. Ji, L.; Li, L.; Ji, X.; Zhang, Y.; Mou, S.; Wu, T.; Liu, Q.; Li, B.; Zhu, X.; Luo, Y.; et al. Highly Selective Electrochemical Reduction of CO_2 to Alcohols on an FeP Nanoarray. *Angew. Chem. Int. Ed.* **2020**, *59*, 758–762. [CrossRef]
53. Chen, P.; Zhang, P.; Kang, X.; Zheng, L.; Mo, G.; Wu, R.; Tai, J.; Han, B. Efficient Electrocatalytic Reduction of CO_2 to Ethane over Nitrogen-Doped Fe_2O_3. *J. Am. Chem. Soc.* **2022**, *144*, 14769–14777. [CrossRef] [PubMed]
54. Kuk, S.K.; Singh, R.K.; Nam, D.H.; Singh, R.; Lee, J.-K.; Park, C.B. Photoelectrochemical Reduction of Carbon Dioxide to Methanol through a Highly Efficient Enzyme Cascade. *Angew. Chem. Int. Ed.* **2017**, *56*, 3827–3832. [CrossRef]
55. Qiu, J.; Zeng, G.; Ha, M.-A.; Ge, M.; Lin, Y.; Hettick, M.; Hou, B.; Alexandrova, A.N.; Javey, A.; Cronin, S.B. Artificial Photosynthesis on TiO_2-Passivated InP Nanopillars. *Nano Lett.* **2015**, *15*, 6177–6181. [CrossRef]
56. Gu, J.; Wuttig, A.; Krizan, J.W.; Hu, Y.; Detweiler, Z.M.; Cava, R.J.; Bocarsly, A.B. Mg-Doped $CuFeO_2$ Photocathodes for Photoelectrochemical Reduction of Carbon Dioxide. *J. Phys. Chem. C* **2013**, *117*, 12415–12422. [CrossRef]
57. Sagara, N.; Kamimura, S.; Tsubota, T.; Ohno, T. Photoelectrochemical CO_2 reduction by a p-type boron-doped g-C_3N_4 electrode under visible light. *Appl. Catal. B Environ.* **2016**, *192*, 193–198. [CrossRef]
58. Jang, Y.J.; Bhatt, M.D.; Lee, J.; Choi, S.H.; Lee, B.J.; Lee, J.S. Metal-Free Artificial Photosynthesis of Carbon Monoxide Using N-Doped ZnTe Nanorod Photocathode Decorated with N-Doped Carbon Electrocatalyst Layer. *Adv. Energy Mater.* **2018**, *8*, 1702636. [CrossRef]
59. Li, W.; Bandosz, T.J. Role of Heteroatoms in S,N-Codoped Nanoporous Carbon Materials in CO_2 (Photo)electrochemical Reduction. *ChemSusChem* **2018**, *11*, 2987–2999. [CrossRef] [PubMed]
60. Kim, Y.; Creel, E.B.; Corson, E.R.; McCloskey, B.D.; Urban, J.J.; Kostecki, R. Surface-Plasmon-Assisted Photoelectrochemical Reduction of CO_2 and NO_3−on Nanostructured Silver Electrodes. *Adv. Energy Mater.* **2018**, *8*, 1800363. [CrossRef]
61. Zhou, W.; Guo, J.-K.; Shen, S.; Pan, J.; Tang, J.; Chen, L.; Au, C.-T.; Yin, S.-F. Progress in Photoelectrocatalytic Reduction of Carbon Dioxide. *Acta Phys. Chim. Sin.* **2020**, *36*, 1906048. [CrossRef]
62. Jang, Y.J.; Jang, J.-W.; Lee, J.; Kim, J.H.; Kumagai, H.; Lee, J.; Minegishi, T.; Kubota, J.; Domen, K.; Lee, J.S. Selective CO production by Au coupled ZnTe/ZnO in the photoelectrochemical CO_2 reduction system. *Energy Environ. Sci.* **2015**, *8*, 3597–3604. [CrossRef]
63. Jang, Y.J.; Jeong, I.; Lee, J.; Lee, J.; Ko, M.J.; Lee, J.S. Unbiased Sunlight-Driven Artificial Photosynthesis of Carbon Monoxide from CO_2 Using a ZnTe-Based Photocathode and a Perovskite Solar Cell in Tandem. *ACS Nano* **2016**, *10*, 6980–6987. [CrossRef] [PubMed]
64. Ghadimkhani, G.; de Tacconi, N.R.; Chanmanee, W.; Janaky, C.; Rajeshwar, K. Efficient solar photoelectrosynthesis of methanol from carbon dioxide using hybrid CuO-Cu_2O semiconductor nanorod arrays. *Chem. Commun.* **2013**, *49*, 1297–1299. [CrossRef] [PubMed]
65. Kang, U.; Choi, S.K.; Ham, D.J.; Ji, S.M.; Choi, W.; Han, D.S.; Abdel-Wahab, A.; Park, H. Photosynthesis of formate from CO_2 and water at 1% energy efficiency via copper iron oxide catalysis. *Energy Environ. Sci.* **2015**, *8*, 2638–2643. [CrossRef]
66. Deng, X.; Li, R.; Wu, S.; Wang, L.; Hu, J.; Ma, J.; Jiang, W.; Zhang, N.; Zheng, X.; Gao, C.; et al. Metal-Organic Framework Coating Enhances the Performance of Cu_2O in Photoelectrochemical CO_2 Reduction. *J. Am. Chem. Soc.* **2019**, *141*, 10924–10929. [CrossRef]
67. Roy, S.; Miller, M.; Warnan, J.; Leung, J.J.; Sahm, C.D.; Reisner, E. Electrocatalytic and Solar-Driven Reduction of Aqueous CO_2 with Molecular Cobalt Phthalocyanine–Metal Oxide Hybrid Materials. *ACS Catal.* **2021**, *11*, 1868–1876. [CrossRef]
68. Hasan, R.; Hamid, S.B.A.; Basirun, W.J. Charge transfer behavior of graphene-titania photoanode in CO_2 photoelectrocatalysis process. *Appl. Surf. Sci.* **2015**, *339*, 22–27. [CrossRef]
69. Llorente, M.; Froehlich, J.; Dang, T.; Sathrum, A.; Kubiak, C.P. Photochemical and Photoelectrochemical Reduction of CO_2. *Annu. Rev. Phys. Chem.* **2012**, *63*, 541–569. [CrossRef]
70. Kaniyankandy, S.; Rawalekar, S.; Verma, S.; Ghosh, H.N. Ultrafast Hole Transfer in CdSe/ZnTe Type II Core−Shell Nanostructure. *J. Phys. Chem. C* **2011**, *115*, 1428–1435. [CrossRef]
71. Jang, J.-W.; Cho, S.; Magesh, G.; Jang, Y.J.; Kim, J.Y.; Kim, W.Y.; Seo, J.K.; Kim, S.; Lee, K.-H.; Lee, J.S. Aqueous-Solution Route to Zinc Telluride Films for Application to CO_2 Reduction. *Angew. Chem. Int. Ed.* **2014**, *53*, 5852–5857. [CrossRef] [PubMed]
72. Huang, X.; Shen, Q.; Liu, J.; Yang, N.; Zhao, G. A CO_2 adsorption-enhanced semiconductor/metal-complex hybrid photoelectrocatalytic interface for efficient formate production. *Energy Environ. Sci.* **2016**, *9*, 3161–3171. [CrossRef]
73. Gasparotto, A.; Barreca, D.; Bekermann, D.; Devi, A.; Fischer, R.A.; Fornasiero, P.; Gombac, V.; Lebedev, O.I.; Maccato, C.; Montini, T.; et al. F-Doped Co_3O_4 Photocatalysts for Sustainable H_2 Generation from Water/Ethanol. *J. Am. Chem. Soc.* **2011**, *133*, 19362–19365. [CrossRef]

74. Huang, X.; Cao, T.; Liu, M.; Zhao, G. Synergistic Photoelectrochemical Synthesis of Formate from CO_2 on {12(1)over-bar} Hierarchical Co_3O_4. *J. Phys. Chem. C* **2013**, *117*, 26432–26440. [CrossRef]
75. Shen, Q.; Chen, Z.; Huang, X.; Liu, M.; Zhao, G. High-Yield and Selective Photoelectrocatalytic Reduction of CO_2 to Formate by Metallic Copper Decorated Co_3O_4 Nanotube Arrays. *Environ. Sci. Technol.* **2015**, *49*, 5828–5835. [CrossRef] [PubMed]
76. Shen, Q.; Huang, X.; Liu, J.; Guo, C.; Zhao, G. Biomimetic photoelectrocatalytic conversion of greenhouse gas carbon dioxide: Two-electron reduction for efficient formate production. *Appl. Catal. B Environ.* **2017**, *201*, 70–76. [CrossRef]
77. Song, J.T.; Ryoo, H.; Cho, M.; Kim, J.; Kim, J.-G.; Chung, S.-Y.; Oh, J. Nanoporous Au Thin Films on Si Photoelectrodes for Selective and Efficient Photoelectrochemical CO_2 Reduction. *Adv. Energy Mater.* **2017**, *7*, 1601103. [CrossRef]
78. Bradley, M.; Tysak, T. p-Type silicon based photoelectrochemical cells for optical energy conversion: Electrochemistry of tetra-azomacrocyclic metal complexes at illuminated. *J. Electroanal. Chem. Interfacial Electrochem.* **1982**, *135*, 153–157. [CrossRef]
79. Choi, S.; Kang, U.; Lee, S.; Ham, D.; Ji, S.; Park, H. Sn-Coupled p-Si Nanowire Arrays for Solar Formate Production from CO_2. *Adv. Energy Mater.* **2014**, *4*, 1301614. [CrossRef]
80. Chu, S.; Fan, S.; Wang, Y.; Rossouw, D.; Wang, Y.; Botton, G.A.; Mi, Z. Tunable Syngas Production from CO_2 and H_2O in an Aqueous Photoelectrochemical Cell. *Angew. Chem. Int. Edit.* **2016**, *55*, 14262–14266. [CrossRef]
81. Read, C.G.; Park, Y.; Choi, K.-S. Electrochemical Synthesis of p-Type $CuFeO_2$ Electrodes for Use in a Photoelectrochemical Cell. *J. Phys. Chem. Lett.* **2012**, *3*, 1872–1876. [CrossRef] [PubMed]
82. Yang, Z.; Xu, J.; Wu, C.; Jing, H.; Li, P.; Yin, H. New insight into photoelectric converting CO_2 to CH_3OH on the one-dimensional ribbon CoPc enhanced Fe_2O_3 NTs. *Appl. Catal. B Environ.* **2014**, *156–157*, 249–256. [CrossRef]
83. Jiang, M.; Wu, H.; Li, Z.; Ji, D.; Li, W.; Liu, Y.; Yuan, D.; Wang, B.; Zhang, Z. Highly Selective Photoelectrochemical Conversion of Carbon Dioxide to Formic Acid. *ACS Sustain. Chem. Eng.* **2017**, *6*, 82–87. [CrossRef]
84. Luo, J.; Steier, L.; Son, M.-K.; Schreier, M.; Mayer, M.T.; Grätzel, M. Cu_2O Nanowire Photocathodes for Efficient and Durable Solar Water Splitting. *Nano Lett.* **2016**, *16*, 1848–1857. [CrossRef] [PubMed]
85. Shi, Y.; Wang, Y.; Dong, C.; Nga, T.T.T.; Wei, D.; Wang, J.; Zhao, X.; Wang, M.; Zhang, K.; Li, M.; et al. Localized Geometry Determined Selectivity of Iodide-Derived Copper for Electrochemical CO_2 Reduction. *Adv. Energy Mater.* **2023**, *13*, 2203896. [CrossRef]
86. Dubale, A.A.; Su, W.-N.; Tamirat, A.G.; Pan, C.-J.; Aragaw, B.A.; Chen, H.-M.; Chen, C.-H.; Hwang, B.-J. The synergetic effect of graphene on Cu_2O nanowire arrays as a highly efficient hydrogen evolution photocathode in water splitting. *J. Mater. Chem. A* **2014**, *2*, 18383–18397. [CrossRef]
87. Paracchino, A.; Laporte, V.; Sivula, K.; Grätzel, M.; Thimsen, E. Highly active oxide photocathode for photoelectrochemical water reduction. *Nat. Mater.* **2011**, *10*, 456–461. [CrossRef]
88. Rajeshwar, K.; De Tacconi, N.R.; Ghadimkhani, G.; Chanmanee, W.; Janáky, C. Tailoring Copper Oxide Semiconductor Nanorod Arrays for Photoelectrochemical Reduction of Carbon Dioxide to Methanol. *ChemPhysChem* **2013**, *14*, 2251–2259. [CrossRef]
89. Li, P.; Jing, H.; Xu, J.; Wu, C.; Peng, H.; Lu, J.; Lu, F. High-efficiency synergistic conversion of CO_2 to methanol using Fe_2O_3 nanotubes modified with double-layer Cu_2O spheres. *Nanoscale* **2014**, *6*, 11380–11386. [CrossRef]
90. Kang, H.-Y.; Nam, D.-H.; Yang, K.D.; Joo, W.; Kwak, H.; Kim, H.-H.; Hong, S.-H.; Nam, K.T.; Joo, Y.-C. Synthetic Mechanism Discovery of Monophase Cuprous Oxide for Record High Photoelectrochemical Conversion of CO_2 to Methanol in Water. *ACS Nano* **2018**, *12*, 8187–8196. [CrossRef]
91. Dong, F.; Wu, L.; Sun, Y.; Fu, M.; Wu, Z.; Lee, S.C. Efficient synthesis of polymeric g-C_3N_4 layered materials as novel efficient visible light driven photocatalysts. *J. Mater. Chem.* **2011**, *21*, 15171–15174. [CrossRef]
92. Hui, X.; Song, Y.; Song, Y.; Zhu, J.; Zhu, T.; Liu, C.; Zhao, D.; Zhang, Q.; Li, H. Synthesis and characterization of g-C_3N_4/Ag_2CO_3 with enhanced visible-light photocatalytic activity for the degradation of organic pollutants. *RSC Adv.* **2014**, *4*, 34539–34547.
93. Wang, Q.; Wang, X.; Yu, Z.; Jiang, X.; Chen, J.; Tao, L.; Wang, M.; Shen, Y. Artificial photosynthesis of ethanol using type-II g-C_3N_4/ZnTe heterojunction in photoelectrochemical CO_2 reduction system. *Nano Energy* **2019**, *60*, 827–835. [CrossRef]
94. Liu, L.; Zhao, H.; Andino, J.M.; Li, Y. Photocatalytic CO_2 Reduction with H_2O on TiO_2 Nanocrystals: Comparison of Anatase, Rutile, and Brookite Polymorphs and Exploration of Surface Chemistry. *ACS Catal.* **2012**, *2*, 1817–1828. [CrossRef]
95. Cardoso, J.C.; Stulp, S.; De Brito, J.F.; Flor, J.B.S.; Frem, R.C.G.; Zanoni, M.V.B. MOFs based on ZIF-8 deposited on TiO_2 nanotubes increase the surface adsorption of CO_2 and its photoelectrocatalytic reduction to alcohols in aqueous media. *Appl. Catal. B Environ.* **2018**, *225*, 563–573. [CrossRef]
96. Cardoso, J.C.; Stulp, S.; de Souza, M.K.; Hudari, F.F.; Gubiani, J.R.; Frem, R.C.G.; Zanoni, M.V.B. The effective role of ascorbic acid in the photoelectrocatalytic reduction of CO_2 preconcentrated on TiO_2 nanotubes modified by ZIF-8. *J. Electroanal. Chem.* **2020**, *856*, 113384. [CrossRef]
97. Zhang, W.; Hu, Y.; Ma, L.; Zhu, G.; Wang, Y.; Xue, X.; Chen, R.; Yang, S.; Jin, Z. Progress and Perspective of Electrocatalytic CO_2 Reduction for Renewable Carbonaceous Fuels and Chemicals. *Adv. Sci.* **2018**, *5*, 1700275. [CrossRef]
98. Kortlever, R.; Shen, J.; Schouten, K.J.P.; Calle-Vallejo, F.; Koper, M.T.M. Catalysts and Reaction Pathways for the Electrochemical Reduction of Carbon Dioxide. *J. Phys. Chem. Lett.* **2015**, *6*, 4073–4082. [CrossRef]
99. Goyal, P.; Hammes-Schiffer, S. Tuning the Ultrafast Dynamics of Photoinduced Proton-Coupled Electron Transfer in Energy Conversion Processes. *ACS Energy Lett.* **2017**, *2*, 512–519. [CrossRef]

100. Costentin, C.; Robert, M.; Savéant, J.-M. Catalysis of the electrochemical reduction of carbon dioxide. *Chem. Soc. Rev.* **2013**, *42*, 2423–2436. [CrossRef]
101. Hammes-Schiffer, S. Theory of Proton-Coupled Electron Transfer in Energy Conversion Processes. *Acc. Chem. Res.* **2009**, *42*, 1881–1889. [CrossRef] [PubMed]

Disclaimer/Publisher's Note: The statements, opinions and data contained in all publications are solely those of the individual author(s) and contributor(s) and not of MDPI and/or the editor(s). MDPI and/or the editor(s) disclaim responsibility for any injury to people or property resulting from any ideas, methods, instructions or products referred to in the content.